Journal of Experimental Botany, Vol. 68, No. 2 pp. 207–223, 2017
doi:10.1093/jxb/erw432 Advance Access publication 21 December 2016
This paper is available online free of all access charges (see http://jxb.oxfordjournals.org/open_access.html for further details)

RESEARCH PAPER

Molecular phylogeny and forms of photosynthesis in tribe Salsoleae (Chenopodiaceae)

Christina Schüssler[1,6], Helmut Freitag[2], Nuria Koteyeva[3], Denise Schmidt[5], Gerald Edwards[4], Elena Voznesenskaya[3] and Gudrun Kadereit[5,*]

[1] Botany Department, State Museum of Natural History Stuttgart, Rosenstein 1, D-70191 Stuttgart, Germany
[2] Institut für Biologie, Universität Kassel, Heinrich-Plett-Str. 40, D-34132 Kassel, Germany
[3] Laboratory of Anatomy and Morphology, V. L. Komarov Botanical Institute of Russian Academy of Sciences, Prof. Popov Street 2, 197376, St. Petersburg, Russia
[4] School of Biological Sciences, Washington State University, Pullman, WA 99164-4236, USA
[5] Institute für Allgemeine und Spezielle Botanik und Botanischer Garten der Johannes Gutenberg-Universität Mainz, D-55099 Mainz, Germany
[6] Centre for Organismal Studies Heidelberg, Biodiversity and Plant Systematics, Heidelberg University, D-69120 Heidelberg, Germany

* Correspondence: clausing@uni-mainz.de

Received 5 June 2016; Editorial decision 31 October 2016; Accepted 4 November 2016

Editor: Susanne von Caemmerer, Australian National University

Abstract

While many C_4 lineages have Kranz anatomy around individual veins, Salsoleae have evolved the Salsoloid Kranz anatomy where a continuous dual layer of chlorenchyma cells encloses the vascular and water-storage tissue. With the aim of elucidating the evolution of C_4 photosynthesis in Salsoleae, a broadly sampled molecular phylogeny and anatomical survey was conducted, together with biochemical, microscopic, and physiological analyses of selected photosynthetic types. From analyses of photosynthetic phenotypes, a model for evolution of this form of C_4 was compared with models for evolution of Kranz anatomy around individual veins. A functionally C_3 proto-Kranz phenotype (Proto-Kranz Sympegmoid) and intermediates with a photorespiratory pump (Kranz-like Sympegmoid and Kranz-like Salsoloid types) are considered crucial transitional steps towards C_4 development. The molecular phylogeny provides evidence for C_3 being the ancestral photosynthetic pathway but there is no phylogenetic evidence for the ancestry of C_3–C_4 intermediacy with respect to C_4 in Salsoleae. Traits considered advantageous in arid conditions, such as annual life form, central sclerenchyma in leaves, and reduction of surface area, evolved repeatedly in Salsoleae. The recurrent evolution of a green stem cortex taking over photosynthesis in C_4 clades of Salsoleae concurrent with leaf reduction was probably favoured by the higher productivity of the C_4 cycle.

Key words: Ancestral character state reconstruction, C_2 pathway, C_3–C_4 intermediates, CO_2 compensation point, leaf anatomy, TEM, western blots.

Introduction

Reconstructing the evolution of C_4 photosynthesis is challenging as it requires the complex coordination of anatomical, ultrastructural, biochemical, and gene regulatory changes from C_3 ancestors (Hibberd and Covshoff, 2010; Gowik and Westhoff, 2011; Sage *et al.*, 2012, 2014; Williams *et al.*, 2012; Hancock and Edwards, 2014). In bringing together these

Abbreviations: BS, bundle sheath in C_3 species; Γ, CO_2 compensation point; GDC, glycine decarboxylase; KC, Kranz cell (for C_4 species); KLC, Kranz-like cell (for C_3–C_4 intermediate phenotypes); M, mesophyll; ML, maximum likelihood; NAD-ME, NAD-malic enzyme; NADP-ME, NADP-malic enzyme; PEPC, phosphoenolpyruvate carboxylase; PPDK, pyruvate, Pi dikinase; VB, vascular bundle; WS, water storage.

aspects, a model of C_4 evolution where Kranz anatomy is formed around individual veins has been developed over the last 30 years, which includes potential evolutionary precursors and a number of transitional, evolutionary-stable states (Monson *et al.*, 1984; Edwards and Ku, 1987; Sage, 2004; Gowik and Westhoff, 2011; Sage *et al.*, 2012, 2014). These hypothetical states are based on distinct phenotypes observed in nature in close relatives of C_4 lineages and are characterized by a combination of C_3 and C_4 characteristics. From these, a stepwise progression from C_3 to proto-Kranz to photosynthetic intermediates, and finally to C_4 photosynthesis was proposed with a progressive reduction in photorespiration (Sage *et al.*, 2014; hereafter named the '*Flaveria* model' based on photosynthetic phenotypes studied in this genus).

In dicots, there are many anatomical forms of Kranz anatomy that differ in the arrangement of a dual layer of chlorenchyma cells performing the C_4 pathway. These includes forms where Kranz anatomy develops around individual veins; however, there are also nine forms where two concentric chlorenchyma layers surround all veins (Edwards and Voznesenskaya, 2011). According to Brown (1975), in C_4 plants we refer to cells of the inner chlorenchyma layer that become specialized for C_4 photosynthesis, irrespective of their position in the leaf, as Kranz cells (KC) and the outer layer as mesophyll (M) cells (Edwards and Voznesenskaya, 2011; Voznesenskaya *et al.*, 2013). In C_3–C_4 intermediate phenotypes the inner layer of chlorenchyma, which has become specialized to support the C_2 cycle, is referred to as Kranz-like cells (KLC; Voznesenskaya *et al.*, 2013). In C_3 species vascular bundles (VB) are surrounded by non-specialized parenchymatic bundle sheath (BS) cells.

Proto-Kranz phenotypes, first described in *Heliotropium* and *Flaveria*, are suggested to represent the initial phase of C_4 evolution where overall vein density is increased and BS cells have an increased number of organelles, with enlarged mitochondria located internally to chloroplasts in a centripetal position towards the VB (Muhaidat *et al.*, 2011; Sage *et al.*, 2012, 2013, 2014). C_3–C_4 intermediate phenotypes, which have been found in grasses and in a number of dicot families, have in common increased development of chloroplasts and mitochondria in the KLCs. Both M and KLC chloroplasts have Rubisco and the C_3 cycle. In the KLCs there is a distinctive layer of mitochondria that are located internally to the chloroplasts in a centripetal position. In C_3–C_4 intermediate phenotypes glycine decarboxylase (GDC) is selectively localized in the KLC mitochondria, which support a C_2 cycle by establishing a photorespiratory CO_2 pump. In the C_2 cycle photorespiratory glycine produced in the M cells is shuttled for decarboxylation by GDC to the KLCs where photorespired CO_2 is concentrated, enhancing its capture by KLC Rubisco (see Edwards and Ku, 1987; Sage *et al.*, 2012, 2014; Voznesenskaya *et al.*, 2013; Khoshravesh *et al.*, 2016).

For the '*Flaveria* model' C_3–C_4 intermediate phenotypes have been classified into two general groups: Type I and Type II C_3–C_4 species (Edwards and Ku, 1987; alternatively called Type 1 C_2 and Type 2 C_2, Sage *et al.*, 2014). Type I C_3–C_4 species have developed little or no capacity for function of a C_4 cycle as activities/quantities of C_4 enzymes are low, similar to C_3 species. These intermediates mainly reduce losses of the CO_2 generated by photorespiration by its partial refixation in the KLCs. Type II intermediates have substantial expression of a C_4 cycle; e.g. the levels of the C_4 cycle enzymes phosphoenolpyruvate carboxylase (PEPC), pyruvate phosphate dikinase (PPDK), and NADP-malic enzyme (NADP-ME) are two- to five-fold higher in Type II C_3–C_4 species than in C_3 species (Ku *et al.*, 1983, 1991; Edwards and Ku, 1987; Moore *et al.*, 1987; Muhaidat *et al.*, 2011; Sage *et al.*, 2012). The values of CO_2 compensation points (Γ) in C_3–C_4 intermediate phenotypes are in between those of C_3 and C_4 species.

The fact that C_3–C_4 intermediate phenotypes thrive, persist, and occasionally have been found in lineages without any C_4 relatives, suggests that they represent an evolutionary-stable condition in their own right (Monson *et al.*, 1984; Edwards and Ku, 1987). Their predominant occurrence close to C_4 groups may be strongly biased by the more intensive screening in these lineages. Thus, C_3–C_4 intermediate phenotypes do not necessarily represent transitional states that always lead to the establishment of C_4 photosynthesis. A C_2 cycle might already be favourable in conditions of high photorespiration, e.g. in hot, dry, and saline environments (Keerberg *et al.*, 2014). The '*Flaveria* model' is functionally plausible, and supported by phenotypes that actually exist in nature (Sage *et al.*, 2014); however, phylogenetic evidence for the ancestry of the C_3–C_4 intermediate condition is scarce, and is hampered by the generally low number of species with intermediate phenotypes.

C_3–C_4 intermediate phenotypes have been recognized in 16 angiosperm genera (Sage *et al.*, 2012, 2014; Khoshravesh *et al.*, 2016). Often, the ancestry of the C_3–C_4 intermediate condition is inferred from a sister-group relationship of a C_4 lineage and a C_3–C_4 intermediate lineage (Sage *et al.*, 2011, 2012) because the intermediate condition is *a priori* considered as less derived. However, in such cases it is impossible to distinguish between ancestry and a *de novo* evolution of the C_3–C_4 intermediate condition (compare with Hancock and Edwards, 2014). If those cases in which C_3–C_4 intermediate photosynthesis seems to precede C_4 photosynthesis, as suggested in Sage *et al.* (2011; 2012), are critically tested for unequivocal phylogenetic evidence, only *Flaveria* (Asteraceae) studied by McKown *et al.* (2005) holds up. In this case, a stepwise acquisition of C_4 photosynthesis in one lineage of *Flaveria* was shown (McKown *et al.*, 2005; Lyu *et al.*, 2015).

There are four other promising groups that are rich in C_3–C_4 intermediate phenotypes and therefore potentially informative lineages in terms of disentangling the steps of C_4 evolution and ancestral state reconstruction for C_3–C_4 intermediacy: *Blepharis* (Fisher *et al.*, 2015), *Anticharis* (Khoshravesh *et al.*, 2012), *Heliotropium* (Sage *et al.*, 2012), and Salsoleae *sensu stricto* (*s.s.*; Voznesenskaya *et al.*, 2013). A better understanding of C_3–C_4 intermediate phenotypes in Salsoleae is particulary important as these, in contrast to the other groups, seem to deviate from the '*Flaveria* model' (see 'Salsoleae model', Voznesenskaya *et al.*, 2013).

Salsoleae, especially the former section *Coccosalsola*, has long been known to contain C_3 and C_4 species (Winter, 1981; Akhani *et al.*, 1997). In fact, Salsoleae has repeatedly been

suspected to contain species that represent reversions from C_4 back to C_3 photosynthesis (Carolin *et al.*, 1975; P'yankov *et al.*, 1997; Kadereit *et al.*, 2014); however, this has been questioned by Kadereit *et al.* (2003). According to a survey by Voznesenskaya *et al.* (2013, see table 5) there are at least 21 species with $\delta^{13}C$ values within the typical range of C_3 species in Salsoleae. So far, four of these have been shown to possess either proto-Kranz (*Salsola montana*), or a C_3–C_4 intermediate phenotype (*S. arbusculiformis*, *S. divaricata*, and *S. laricifolia* (Voznesenskaya *et al.*, 2013 and references therein; Wen and Zhang, 2015). In the '*Flaveria* model' Kranz anatomy is formed around individual veins, requiring a series of anatomical changes in progression from C_3 to C_4. In Salsoleae, however, the photosynthetic tissue in leaves forms a continuous layer that surrounds all the vascular and water-storage tissue, i.e. in C_3 species by multiple layers of mesophyll tissue (Sympegmoid-type anatomy), and in C_4 species by a dual layer of chlorenchyma tissue forming a Kranz anatomy (Salsoloid-type anatomy). Voznesenskaya *et al.* (2013) proposed a model for transitions from C_3 to proto-Kranz to C_3–C_4 intermediates to C_4 in Salsoleae, based on limited photosynthetic phenotypes, which would require very different changes in leaf anatomy and regulation of development of the dual layer of chlorenchyma cells compared to that in the '*Flaveria* model' for development of Kranz anatomy around individual veins.

Here, we conduct a large-scale analysis of Salsoleae, including species with C_3-type $\delta^{13}C$ values. The results of a molecular phylogenetic study of 74 species and an anatomical survey of 77 species of Salsoleae *s.s*, and some outgroup species, are presented. Furthermore, in a search for additional C_3–C_4 intermediates in the tribe, anatomical, ultrastructural, enzyme content, and gas exchange analyses were performed on a number of species that have C_3-type $\delta^{13}C$ values. Molecular clock and character optimization analyses were used to reconstruct the evolution of the C_4 pathway in Salsoleae. The following questions were addressed. (1) Is there evidence for additional C_3–C_4 intermediates in Salsoleae? (2) What is the current model for evolution of C_4 in Salsoleae based on analyses of photosynthetic phenotypes? (3) In what ways does this model differ from the '*Flaveria* model' proposed in Sage *et al.* (2012, 2014)? (4) Where and when did C_4 photosynthesis originate in Salsoleae, and is there phylogenetic evidence for a reversion from C_4 back to C_3? (5) Does the C_3–C_4 intermediate condition represent an ancestral state to C_4 in Salsoleae?

Material and methods

Plant material and sampling

Species and samples included in the analyses with their respective voucher information are listed in Supplementary Table S1 at *JXB* online. We used herbarium samples and plants grown in the greenhouse at the Botanical Gardens of the University of Mainz, Germany, and at Washington State University (WSU), Pullman, WA, USA, and leaves of specimens that were fixed during various expeditions, mainly by H. Freitag. A few samples were kindly provided by other institutions. Species of the *Kali* clade were mostly left out, because in the trees based on chloroplast sequence data they are separated from the Salsoleae *s.s.*

In WSU, plants were grown in 15-cm diameter pots with commercial potting soil in a growth chamber (model GC-16; Enconair Ecological Chambers Inc., Winnipeg, Canada) under a 14/10 h 25/18 °C day/night cycle under mid-day PPFD of ~500 µmol quanta m^{-2} s^{-1}, and 50% relative humidity for ~2 months. Plants were watered daily and fertilized once per week with Peter's Professional fertilizer (20:20:20 Scotts Miracle-Gro, Marysville, OH, USA).

Our sampling of Salsoleae for the molecular phylogenetic analyses comprised 74 species representing all currently accepted genera (Supplementary Table S2) and included 15 species with C_3-like carbon isotope ($\delta^{13}C$) values (compare with table 5 in Voznesenskaya *et al.*, 2013). Furthermore, representatives of other primary clades of Salsoloideae (Supplementary Table S2) as well as representatives of Camphorosmoideae were included. For rooting and dating purposes Suaedoideae and Salicornioideae were sampled as outgroups (Supplementary Table S1). For light microscopy 77 species were examined, mostly from the same material (Supplementary Table S1), including 34 species studied for the first time. Data for eight species were taken from the literature. Six species having different anatomical types (most not previously known in that respect) were chosen for study by electron microscopy, and $\delta^{13}C$, *in situ* immunolocalization, western blot, and gas exchange analyses.

With respect to nomenclature, apart from a few exceptions we follow previous accounts of the different subfamilies, in particular Botschantzev (1989), Akhani *et al.* (2007), and Kadereit and Freitag (2011), although we are aware that more nomenclatural adjustments are required.

Sequencing and phylogenetic inference

Total DNA was extracted from dried or fresh leaf material using the DNeasy Plant Mini Kit (QIAGEN, Germany) or innuPREP Plant DNA Kit (Analytik Jena, Germany) following the manufacturers' protocols but increasing incubation times. PCRs for five markers (*atpB-rbcL* intergenic spacer, *ndhF-rpL32* spacer, *trnQ-rps16* spacer, *rpl16* intron, ITS) were carried out in a T-Professional or T-Gradient Thermocycler (Biometra, Germany), or a PTC100 Thermocycler (MJ Research, USA). Primers sequences, PCR recipes, and cycler programs are documented in Supplementary Table S3. PCR products were checked on 0.8% agarose gels and purified using the NucleoSpin® Gel and PCR clean-up-Kit (Macherey-Nagel, Germany) or ExoSAP (Affymetrix, USA) following the manufacturers' instructions. The Big Dye® Terminator v3.1 Cycle Sequencing Kit (Applied Biosystems) combined with the primers mentioned above was used for the sequencing reactions, followed by a purification step using IllustraTM SephadexTM G-50 Fine DNA Grade (GE Healthcare, UK). Sequencing was performed following the Sanger method on a 3130xI Genetic Analyzer (Applied Biosystems Inc., USA). The raw forward and reverse sequences were checked and automatically aligned in Sequencher 4.1.4 (Gene Codes Corporation, USA). The refined alignment was performed in Mesquite 2.75 (http://mesquiteproject.org) and carefully checked visually. The program SequenceMatrix (v. 1.7.8; Vaidya *et al.*, 2011) was used to combine the four chloroplast (cp) marker data sets.

Phylogenetic analyses under the settings outlined below were initially conducted individually for the five selected DNA regions. Results of the individual analyses of the four cp markers revealed no topological conflict [i.e. incongruence with ML Bootstrap ≥65% and Posterior Probability (PP) ≥0.90] among individual markers and combination of the cp markers distinctly increased the resolution and support values. For the cp data further analyses were performed using two large and different data sets: (1) a data set with 106 taxa (106t data set) including a broad outgroup sampling; and (2) a data set with 75 taxa (75t data set) in which only *Salsola genistoides* served as the outgroup. The 106t data set was used to reveal primary clades in Salsoloideae and for estimation of divergence time, whereas the 75t data set was used for character optimization (see below). Since the ITS tree and the cp tree showed supported conflict at basal branches, and the combination of cp data and ITS for the 75t data set led to a

significant decrease of resolution and support values in some parts of the tree, we concentrated on the cp tree for further analyses and only include the ITS tree for comparison. First, the best-fitting substitution model for the combined cp data sets was inferred using jModelTest (Posada, 2008). CIPRES (Cyberinfrastructure for Phylogenetic Research) Science Gateway V. 3.3. ML phylogenetic analyses were performed using RAxML (Stamatakis, 2006; Stamatakis *et al.*, 2008), including bootstrapping that was halted automatically following the majority-rule 'autoMRE' criterion. Bayesian inference (BI) analysis was conducted using BEAST (Bayesian Evolutionary Analysis by Sampling Trees v.1.8.2; Drummond and Rambaut, 2007) with GTR+G (general time-reversible; best-fitting according to jModeltest under AIC criterion) with a gamma-distribution in four categories as the substitution model. A birth-and-death demographic model was used as the tree prior. Markov Chain Monte Carlo (MCMC) analysis was performed with the following settings: randomly generated starting tree, 20 000 000 (106t data set) or 10 000 000 iterations (75t data set), discarded burn-in of 10%, and sampling every 1000 steps (totalling 10 000). For the 106t data set a relaxed clock model was implemented in which rates for each branch are drawn independently from an exponential distribution (Drummond *et al.*, 2006). The crown node of Salsoloideae and Camphoromoideae was set to 47.0–25.5 mya based on divergence-time estimates in the Chenopodiaceae/Amaranthaceae complex (Kadereit *et al.*, 2012). We assumed a uniform distribution within the age bounds set. Other settings were left in default.

Light and electron microscopy

For light microscopy, after routine checks by manual sectioning, the middle parts of well-developed leaves were selected for transections by a rotary microtome (Leitz 1515). The semi-thin sections of material fixed in FAA [2% (v/v) formaldehyde, 0.5% (v/v) acetic acid, 70% (v/v) ethanol] were studied under a Dialux 20 (Leitz, Wetzlar). Some were first examined and photographed in water to get a better contrast between lignified (blue) and non-lignified (purple) cell walls before embedding into Depex (Serva) for documentation. For detailed study, middle parts of fully developed leaves were fixed and processed in a similar way to that described in Voznesenskaya *et al.* (2013).

For screening purposes, leaf samples from herbarium specimens were first boiled for about 1–3 minutes and hand-cut sections were preserved in glycerol–gelatin. Selected samples for microtome transections were soaked in a 10% solution of NH_3 for 10 d, dehydrated in ethanol, and embedded in Technovit 7100 (Heraeus Kulzer). The samples were sectioned at 5–20 µm using a rotary microtome. Sections were stained in a 6:6:5:6 mixture of Azur II, Eosin Y, methylene blue, and distilled water and mounted in Eukitt (O. Kindler) after drying. Images of the sections were taken using a Leitz Diaplan light microscope combined with Leica Application Suite 2.8.1.

For ultrastructural characterization, ultra-thin sections were taken from the same samples prepared for the light microscopy study and embedded in Spurr's resin as described in Voznesenskaya *et al.* (2013). The number and sizes of mitochondria in chlorenchyma cells were estimated per cell section (about 10–15 cell images from 2–3 separate leaf samples) using an image analysis program (ImageJ 1.37v, https://imagej.nih.gov/ij/index.html).

$\delta^{13}C$ values

Carbon isotope composition of plant samples was determined at Washington State University using a standard procedure relative to PDB (Pee Dee Belemnite) limestone as the carbon isotope standard (Bender *et al.*, 1973). Leaf samples (from plants growing in the WSU growth chamber) were dried at 60 °C for 24 h, and then 1–2 mg were placed in a tin capsule and combusted in a Eurovector elemental analyser. The resulting N_2 and CO_2 gases were separated by gas chromatography and admitted into the inlet of a Micromass Isoprime isotope ratio mass spectrometer (IRMS) for determination of $^{13}C/^{12}C$ ratios (R). $\delta^{13}C$ values were determined where $\delta = 1000 \times (R_{sample}/R_{standard}) - 1$.

In situ *immunolocalization*

Sample preparation and immunolocalization by transmission electron microscopy (TEM) were carried out according to Voznesenskaya *et al.* (2013). The antibody used (raised in rabbit) was against the P subunit of glycine decarboxylase (GDC) from *Pisum sativum* L. (courtesy of D. Oliver, Iowa State University). Pre-immune serum was used for controls. The density of labeling was determined by counting the gold particles on electron micrographs and calculating the number per unit area (µm^2) using ImageJ 1.37v. For each cell type, replicate measurements were made on parts of cell sections (n = 10–15 cell images). Immunolabeling procedures were performed separately for different species; the difference in the labeling intensity reflects the difference between cell types but not between species. The level of background labeling was low in all cases.

Western blot analysis

Extraction of total soluble proteins, protein separation, and blotting onto a nitrocellulose membrane were carried out according to Voznesenskaya *et al.* (2013). A loading control with protein samples (20 µg) separated by 10% (w/v) SDS-PAGE can be found in Supplementary Fig. S1. Western blots were performed using anti-*Amaranthus hypochondriacus* NAD-malic enzyme (NAD-ME) IgG, which was prepared against the 65-kDa α subunit (courtesy of J. Berry; Long and Berry, 1996) (1:5000), anti-*Zea mays* 62-kDa NADP-malic enzyme (NADP-ME) IgG (courtesy of C. Andreo; Maurino *et al.*, 1996) (1:5000), anti-*Zea mays* PEPC IgG (1:100 000), and anti-*Zea mays* pyruvate,Pi dikinase (PPDK) IgG (courtesy of T. Sugiyama) (1:5000). The intensities of bands in western blots were quantified using ImageJ 1.37v and expressed relative to the level in the C_4 species *S. oppositifolia*, which was set at 100%.

CO_2 compensation point

Measurements of CO_2 compensation points (Γ) were made on an individual lateral branch using a Li-Cor lighted chamber (LI-6400-22L; Li-Cor Biosciences, Lincoln, NE, USA) designed for terete or semi-terete conifer leaves. For each species, a part of a branch of an intact plant was enclosed in the chamber and illuminated with a PPFD of 1000 µmol quanta m^{-2} s^{-1} under 400 µmol mol^{-1} CO_2 at 25 °C until a steady-state rate of CO_2 fixation was obtained (generally 45–60 min). For varying CO_2 experiments, the CO_2 level was first decreased, and then increased up to 400 µmol mol^{-1} at 5 min intervals. Γ was determined by extrapolation of the initial slope of rate of CO_2 fixation (A) versus the intercellular CO_2 concentration in the leaf (C_i) through the x-axis where the net rate of CO_2 assimilation equals zero. The leaf area exposed to the incident light was calculated by taking a digital image of the part of the branch that was enclosed in the chamber, and then determining the exposed leaf area using ImageJ 1.37v.

Statistical analysis

Where indicated, standard errors were determined, and ANOVA was performed using Statistica 7.0 software (StatSoft, Inc.). Tukey's HSD (honest significant difference) test was used to analyze differences between amounts of gold particles in BS/KLC/KC versus M for each species, and $\delta^{13}C$ and Γ values in different species. All analyses were performed at the 95% significance level.

Character coding and analyses of character evolution

Analyses of character evolution were conducted for five traits: (1) type of photosynthesis; (2) KC/KLC function; (3) life form; (4) leaf sclerenchyma; and (5) leaf reduction (Table 1). Traits were optimized over 1000 trees of 74 Salsoleae and *Salsola genistoides* as the outgroup obtained in a Bayesian analysis (see above) using the ML criterion in Mesquite (http://mesquiteproject.org). The fit of single- versus two-rate models was tested for traits with two character states using a likelihood ratio test. Table 1 gives information about the coding of the character states of the five traits.

Table 1. *Traits of photosynthetic pathway, leaf anatomy and life form in Salsoleae s.s.*

Trait 1: type of photosynthesis according to carbon isotope value; coding trait 2: C_3 = 0, C_4 = 1. **Trait 2: function of bundle sheath (BS), Kranz-like (KLC) and Kranz cells (KC); coding trait 2:** C_3 type BS cells around peripheral VB (few or no organelles) = 0, KLC with increased number of organelles mostly in centripetal position, GDC only expressed in KLC cells, C_3-C_4 species = 1, C_4 type Kranz cells = 2. **Trait 3: Life form** according to standard floras and our own observations in the field; **coding trait 3:** perennial l = 0, annual = 1. **Trait 4: presence of sclerenchyma** by replacement of major parts of the central water storage tissue; **coding trait 4:** no = 0, yes = 1. **Trait 5: sites of major photosynthetic function; coding trait 5:** predominantly in leaves and leaf-like structures (0), ± equally in leaves and stems (1), predominantly in stems due to reduction of leaves or their trans-formation into thorns (2). References for photosynthetic pathway and leaf anatomy see below table. Species are classified according to carbon isotope composition of leaf tissue as C_3 or C_4. Species are classified as C_3, proto-kranz, C_3-C_4 intermediates, and C_4 based on analyses of leaf anatomy, Trait 2 and C isotope composition, (see text).

Species of Salsoleae *s.s.*	Isolate no. for molecular analysis	Trait 1: Type of photosynthesis according to carbon isotope ratio	Leaf anatomy; type names according to Voznesenskaya *et al.* (2013)	Trait 2	Trait 3	Trait 4	Trait 5
Anabasis aphylla L.	chen 2743/2017	C_4 (1, 2, 12)	salsoloid+H (1, 6, 8, this study)	2	0	0	2
Anabasis articulata (Forssk.) Moq.	chen 2360	C_4 (7)	salsoloid+H (6, 8, 12, this study)	2	0	0	2
Anabasis brevifolia C.A. Mey.	chen 2407	C_4 (12)	salsoloid+H (2, 11, this study)	2	0	0	1
Anabasis calcarea (Charif & Aellen) Bokhari & Wendelbo	chen 1841	C_4 (1)	salsoloid+H (1, this study)	2	0	0	2
Anabasis ehrenbergii Schweinf. ex Boiss.	chen 2403/2741	C_4 (12)	salsoloid+H (this study)	2	0	0	2
Anabasis setifera Moq.	chen 2373	C_4 (7)	salsoloid+H (1, 2, 6, 12, this study)	2	0	0	1
Arthrophytum betpakdalense Korov.	chen 0229	C_4 **	salsoloid+H (this study)	2	0	0	1
Arthrophytum gracile Aellen	chen 2603	C_4 (1)	salsoloid+H (this study)	2	0	0	2
Arthrophytum lehmannianum Bunge	chen 2637	C_4 (4)	salsoloid+H (5, this study)	2	0	0	1
Cornulaca amblyacantha Bunge	chen 0350	C_4 **	salsoloid+H+S (this study)	2	0	1	1
Cornulaca monacantha Delile	chen 0212	C_4 (1, 12)	salsoloid+H+S (2, this study)	2	0	1	1
Cornulaca setifera (DC.) Moq	chen 0304	C_4 (12)	salsoloid+H+S (6, this study)	2	0	1	1
Cyathobasis fruticulosa (Bunge) Aellen	chen 0082	C_4 (12)	salsoloid+H+S (this study)	2	0	1	2
Girgensohnia diptera Bunge	chen 2639	C_4 **	salsoloid+H+S (this study)	2	1	1	2
Girgensohnia minima E. Korov.	chen 2601	C_4 **	salsoloid+H+S (this study)	2	1	1	2
Girgensohnia oppositiflora (Pall.) Fenzl	chen 0033	C_4 (1, 12)	salsoloid+H+S (2, 6, this study)	2	1	1	(1)2
Gyroptera gillettii Botsch	chen 2819	C_4 **	salsoloid+H (this study)	2	0	0	0
Halogeton alopecuroides (Delile) Moq.	chen 0300	C_4 (1, 7, 12)	salsoloid+H (6, 8, 12, this study)	2	0	1	0
Halogeton arachnoideus Moq.	chen 2605	C_4 (1)	salsoloid+H (this study)	2	1	0	0
Halogeton glomeratus (M. Bieb.) C.A. Mey.	chen 0030	C_4 (1)	salsoloid+H (2)	2	1	0	0
Halogeton sativus (L.) Moq.	chen 1229	C_4 (1)	salsoloid+H (8, this study)	2	1	0	0
Halothamnus bottae Jaub. & Spach	chen 0351	C_4 (12)	salsoloid (7)	2	0	0	2
Halothamnus ferganensis Botsch.	chen 0197	C_4 **	salsoloid (7)	2	0	0	1
Halothamnus iliensis (Lipsky) Botsch.	chen 2668	C_4 (1, 12)	salsoloid (7)	2	1	0	1
Halothamnus somalensis (N.E. Br.) Botsch.	chen 2584	C_4 **	salsoloid (7)	2	0	0	2
Haloxylon ammodendron (C.A. Mey.) Bunge	chen 0035	C_4 (1, 2, 12)	salsoloid+H (11, this study)	2	0	0	2
Haloxylon persicum Bunge ex Boiss.	chen 2815	C_4 (7, 12)	salsoloid+H (11)	2	0	0	2
Hammada articulata (Moq.) O. Bolos & Vigo	chen 0196	C_4 **	salsoloid+H (2, 6, this study))	2	0	0	2
Hammada eriantha Botsch.	chen 2813	C_4 **	salsoloid+H (this study)	2	0	0	2
Hammada griffithii (Moq.) Iljin	chen 2635	C_4 (1, 12)	salsoloid+H+S (this study)	2	0	1	2
Hammada negevensis Iljin & Zoh.	chen 2814	C_4 (7, 12)	salsoloid+H (this study)	2	0	0	2
Hammada salicornica (Moq.) Iljin	chen 2752	C_4 (1, 7)	salsoloid+H (2, 8, 12, this study)	2	0	0	2
Hammada schmittiana (Pomel) Botsch.	chen 2629	C_4 (7, 12)	salsoloid+H (this study)	2	0	0	2
Hammada thomsonii (Bunge) Iljin	chen 0178	C_4 **	salsoloid+H+S (this study)	2	0	1	2
Horaninowia capitata Sukhor.	chen 0188	C_4 **	salsoloid+H+S (this study)	2	1	1	1
Horaninowia platyptera Charif & Aellen	chen 2602	C_4 (1)	salsoloid+H+S (this study)	2	1	1	1
Horaninowia ulicina Fisch. & C.A. Mey.	chen 2589	C_4 (1)	salsoloid+H+S (15, this study)	2	1	1	1
Iljinia regelii (Bunge) Korovin	chen 0182	C_4 (4)	salsoloid+H (11, this study)	2	0	0	0
Lagenantha cycloptera (Stapf) M.G. Gilbert & Friis	chen 2809	C_4 **	salsoloid+H (this study)	2	0	0	0
Noaea minuta Boiss. & Bal.	chen 0079	C_4 (12)	salsoloid+S (this study)	2	1	1	0
Noaea mucronata (Forssk.) Asch. & Schweinf.	chen 0019	C_4 (1, 2, 7)	salsoloid+S (6, 9, this study)	2	0	1	(1)2
Nucularia perrinii Batt.	chen 2627	C_4 **	salsoloid+H (8, this study)	2	0	0	0

Table 1. *Continued*

Species of Salsoleae *s.s.*	Isolate no. for molecular analysis	Trait 1: Type of photosynthesis according to carbon isotope ratio	Leaf anatomy; type names according to Voznesenskaya *et al.* (2013)	Trait 2	Trait 3	Trait 4	Trait 5
Rhaphidophyton regelii (Bunge) Iljin	chen 0075	C_3 (4)	kranz-like salsoloid+S (this study)	1	0	1	0
Salsola abrotanoides Bunge	chen 2996	C_3 (4, 6, 9)	sympegmoid (11, this study)	0	0	0	0
Salsola acutifolia (Bunge) Botsch.	chen 2640	C_4 (1, 12)	salsoloid+H (this study)	2	1	0	0
Salsola arbusculiformis Drob.	chen 0176	C_3 (1, 2, 6, 8, 11)	kranz-like sympegmoid (13, 16, this study)	1	0	0	0
Salsola botschantzevii Kurbanov	chen 2630	C_3 (9)	proto-kranz sympegmoid (this study)	0	0	0	0
Salsola cyrenaica (Maire & Weiller) Brullo	chen 0354	C_4 (9)	salsoloid+H (3, this study)	2	0	0	0
Salsola deschaseauxiana Litard. & Maire	chen 2758 (= 2641)	C_3 (9)	kranz-like salsoloid (this study)	1	0	0	0
Salsola divaricata Masson ex Link	chen 2779	C_3 (6, 9)	kranz-like salsoloid (14, this study)	1	0	0	0
Salsola drobovii Botsch.	chen 0175	C_3 (4, 6, 9)	proto-kranz sympegmoid (this study)***	0	0	0	0
Salsola florida (M. Bieb.) Poir.	chen 2811	C_4 (1, 12)	salsoloid+H (2, 6, this study)	2	1	0	0
Salsola foliosa (L.) Schrad.	chen 0103	C_4 (1)	salsoloid+H (11, this study)	2	1	0	0
Salsola grandis Freitag, Vural & N. Adıgüzel	chen 0105	C_4 **	salsoloid+H (4, this study)	2	1	0	0
Salsola gymnomaschala Maire	chen 0355	C_3 (9)	kranz-like salsoloid (this study)	1	0	0	0
Salsola junatovii Botsch.	not included	C_3 (9)	proto-kranz sympegmoid (this study)	0	0	0	0
Salsola kerneri (Woł.) Botsch.	chen 2642	C_4 (1, 6)	salsoloid+H (this study)	2	0	0	0
Salsola laricifolia Turcz. ex Litv.	chen 1355	C_3 (6, 9, 10, 11)	kranz-like salsoloid (14, 15, 16, this study)	1	0	0	0
Salsola lipschitzii Botsch.	not included	C_3 (9)	proto-kranz sympegmoid (this study)	0	0	0	0
Salsola melitensis Botsch.	chen 2644	C_4 (9)	salsoloid+H (this study)	2	0	0	0
Salsola montana Litv.	chen 2591	C_3 (1, 2, 5, 6, 9)	proto-kranz sympegmoid (14)	0	0	0	0
Salsola oppositifolia Desf.	chen 0099	C_4 (1, 6, 9, 12)	salsoloid+H (8, this study)	2	0	0	0
Salsola oreophila Botsch.	chen 2847	C_3 (5, 9)	sympegmoid (10, this study)	0	0	0	0
Salsola pachyphylla Botsch.	chen 2762	C_3 (5, 6)	sympegmoid (11, this study))	0	0	0	0
Salsola rosmarinus (Ehrenb. ex Boiss.) Akhani	chen 0303	C_4 (1, 7)	salsoloid+H (2, 6, this study)	2	0	0	0
Salsola schweinfurthii Solms-Laub.	chen 2827	C_4 (1, 6, 7, 12)	salsoloid+H (this study)	2	0	0	0
Salsola soda L.	chen 2834	C_4 (1, 7)	salsoloid+H (9, this study)	2	1	0	0
Salsola stocksii Boiss.	chen 2646	C_4 (1)	salsoloid+H (2)	2	0	0	1
Salsola tianschanica Botsch.	not included	C_3 (9)	sympegmoid (this study)	0	0	0	0
Salsola tunetana Brullo	chen 2647	C_4 **	salsoloid+H (this study)	2	0	0	0
Salsola verticillata Schousboe	chen 2648	C_3 (this study)*	kranz-like salsoloid (this study)	1	0	0	0
Salsola webbii Moq.	chen 2828	C_3 (1, 6, 9, 12)	sympegmoid (2, 8, 14, this study)	0	0	0	0
Salsola zygophylla Batt. & Trab.	chen 2756	C_4 (1, 6, 12)	salsoloid+H (this study)	2	0	0	0
Salsola zygophylloides (Aellen & Townsend) Akhani	chen 2593	C_4 **	salsoloid+H (this study)	2	0	0	0
Sevada schimperi Moq.	chen 2590	C_4 (3)	salsoloid+H (this study)	2	0	0	0
Sympegma regelii Bunge	chen 383a/2766	C_3 (4, 11)	sympegmoid (2, 9, 16, this study)	0	0	0	0
Salsola genistoides Juss. ex Poir. (outgroup)	chen 1155/1362	C_3 (1, 9)	sympegmoid (11, this study)	0	0	0	2

References for C_3 versus C_4 type carbon isotope ratio: 1 = Akhani *et al.* (1997), 2 = Akhani and Ghasemkhani (2007), 3 = Carolin *et al.* (1975), 4 = Freitag and Stichler (2000), 5 = P'yankov *et al.* (1997), 6 = Pyankov *et al.* (2001), 7 = Shomer-Ilan *et al.* (1981), 8 = Voznesenskaya *et al.* (2001), 9 = Voznesenskaya *et al.* (2013), 10 = Wen and Zhang (2011), 11 = Wen and Zhang (2015), 12 = Winter (1981).
References for leaf anatomy: 1 = Bokhari and Wendelbo (1978), 2 = Carolin *et al.* (1975), 3 = Freitag and Duman (2000), 4 = Freitag *et al.* (1999), 5 = Freitag and Stichler (2000), 6 = Khatib (1959), 7 = Kothe-Heinrich (1993), 8 = Maire (1962), 9 = Monteil (1906), 10 = P'yankov *et al.* (1997), 11 = Pyankov *et al.* (2001), 12 = Volkens (1887), 13 = Voznesenskaya *et al.* (2001), 14 = Voznesenskaya *et al.* (2013), 15 = Wen and Zhang (2011), 16 = Wen and Zhang (2015).
* In Voznesenskaya *et al.* (2013) this species was mentioned to have the C_4 pathway. However, samples for the carbon isotope value were taken from a wrongly identified specimen [D. Podlech 44954 (P)]. The correct identification for this specimen is *Salsola oppositifolia*, which indeed is a C_4 species.
** C_4 metabolism deduced from leaf anatomy, no carbon isotope values available.
*** Classified as sympegmoid in Freitag and Duman (2000), Pyankov *et al.* (2001) and Khatib (1959).

Results

Leaf anatomy

Light microscopy

Figure 1A shows that *S. abrotanoides* (C_3) mostly had two layers of palisade M cells. The peripheral vascular bundles (VBs) were surrounded by a layer of bundle sheath (BS) cells, which looked similar to the adjacent cells of the water-storage (WS) tissue but were smaller.

Four species (all C_3–C_4), *R. regelii*, *S. deschaseauxiana*, *S. gymnomaschala*, and *S. verticillata* (Fig. 1B–E) were similar in having two layers of chlorenchyma cells underneath the epidermis. While the inner layer consisted of elongated palisade cells (M2), the cells of the outer layer (M1) were 2–5 times shorter with a reduction to varying degrees in the number of chloroplasts depending on species and growth conditions. In *R. regelii* the M1 cells were elongated (Figs 1B and 2), but in the other species the M1 cells appeared almost globular to polyhedral in shape; they were wider than the M2 palisade cells and more similar to the typical hypodermis of C_4 species (Fig. 1C–E). These species had a clearly defined continuous (or almost continuous in *R. regelii*) layer of chlorenchymatous Kranz-like cells (KLCs), which was situated above and between the peripheral VBs.

In *S. oppositifolia* (C_4) the palisade M2 cells were rather short and M1 cells were represented by a typical hypodermis consisting of large globular cells that were almost devoid of chloroplasts. The KCs had organelles in a centripetal position; they formed a continuous layer just beneath the palisade cells (Fig. 1F).

Among the *Salsola* species in this study, C_3 *S. abrotanoides* had the lowest volume of WS tissue. In *R. regelii*, the inner part of the WS tissue was replaced by massive sclerenchyma tissue, which accounted for half of the leaf diameter and for

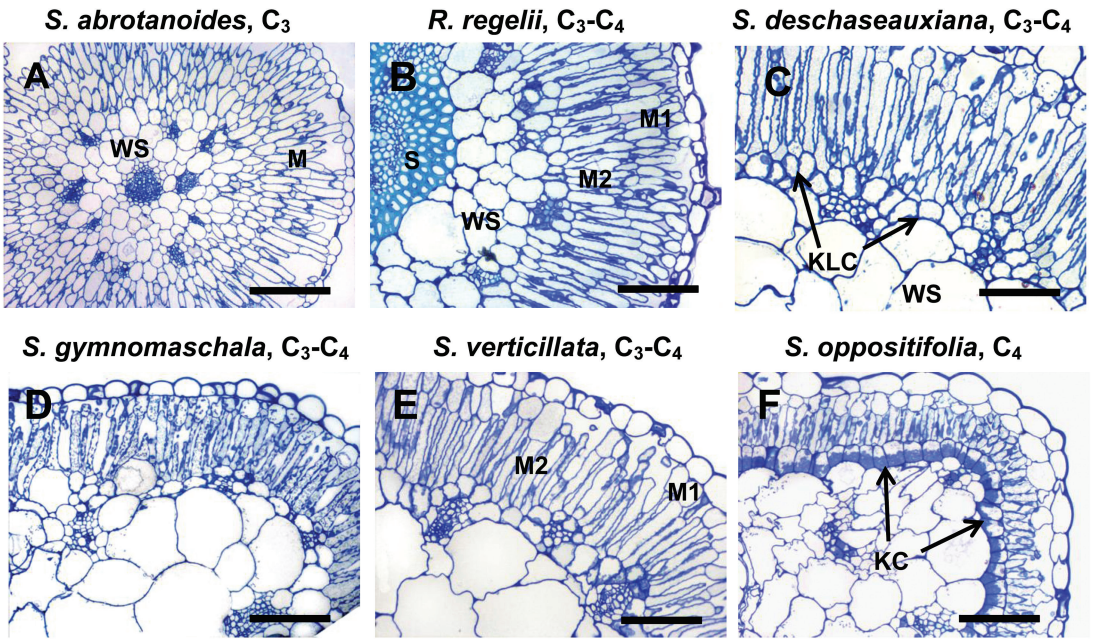

Fig. 1. General anatomy in leaves of five *Salsola* species (A, C–F) and *Rhaphidophyton regelii* (B). *Salsola abrotanoides* (A), *S. deschaseauxiana* (C), *S. gymnomaschala* (D), *S. verticillata* (E), and *S. oppositifolia* (F). The images show light microscopy on leaf cross-sections illustrating the position of the palisade mesophyll (M) and bundle sheath (BS)/Kranz-like cells (KLCs)/Kranz cells (KCs). Note the continuous layer of KLCs in *R. regelii*, *S. deschaseauxiana*, *S. gymnomaschala*, and *S. verticillata*, and the difference between the outer (M1) and inner (M2) layers of mesophyll. Sclerenchyma (S) and water-storage (WS) tissue are also indicated. Scale bars = 200 μm for (A); 100 μm for (B–F).

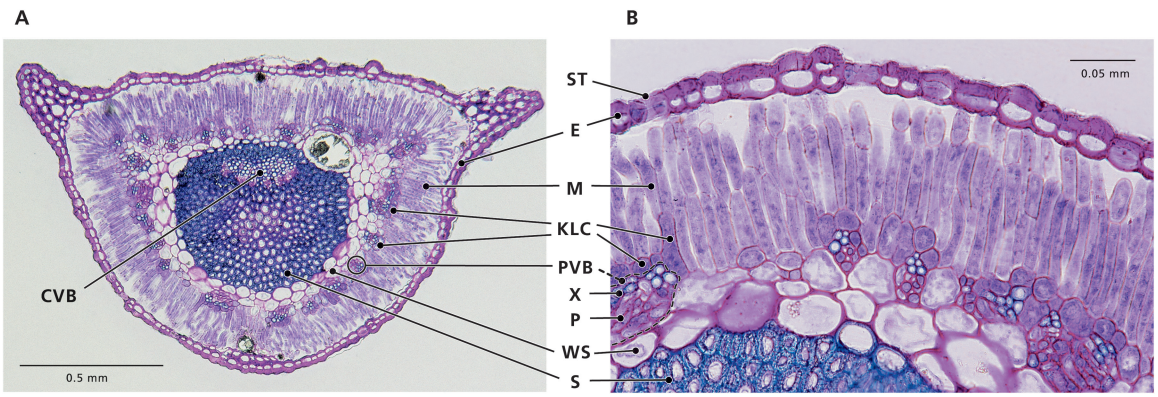

Fig. 2. Leaf cross-sections of *Rhaphidophyton regelii*, a C_3–C_4 species with Kranz-like Salsoloid leaf anatomy. (A) Cross-section of entire leaf, and (B) close-up of the chlorenchyma. Abbreviations: E, epidermis; M, mesophyll; KLC, Kranz-like cells; WS, water storage tissue; S, sclerenchyma; CVB, central vascular bundle; PVB, peripheral vascular bundles; X, xylem; P, phloem; ST, stoma.

the stiff appearance of the leaves (Fig. 2). Crystal-bearing idioblasts were preferentially located in the hypodermis or hypodermis-like layer, and in the Kranz-like layer between the peripheral bundles, but they could occur scattered elsewhere. In *S. gymnomaschala* and in *S. verticillata* the epidermis was partially doubled. In all *Salsola* species the main vein was located more or less in the center of the leaf and surrounded by 2-4 layers of WS tissue.

Transmission electron microscopy

Figure 3 shows obvious differences in the quantity, position, size, and level of development of BS cell organelles in the C_3 species and in the corresponding KLCs in intermediates and the KCs of the C_4 species.

C_3 *Salsola abrotanoides* (Fig. 3A, B) had the lowest number of organelles in BS cells; a few chloroplasts and mitochondria were distributed more or less evenly along the cell wall, with

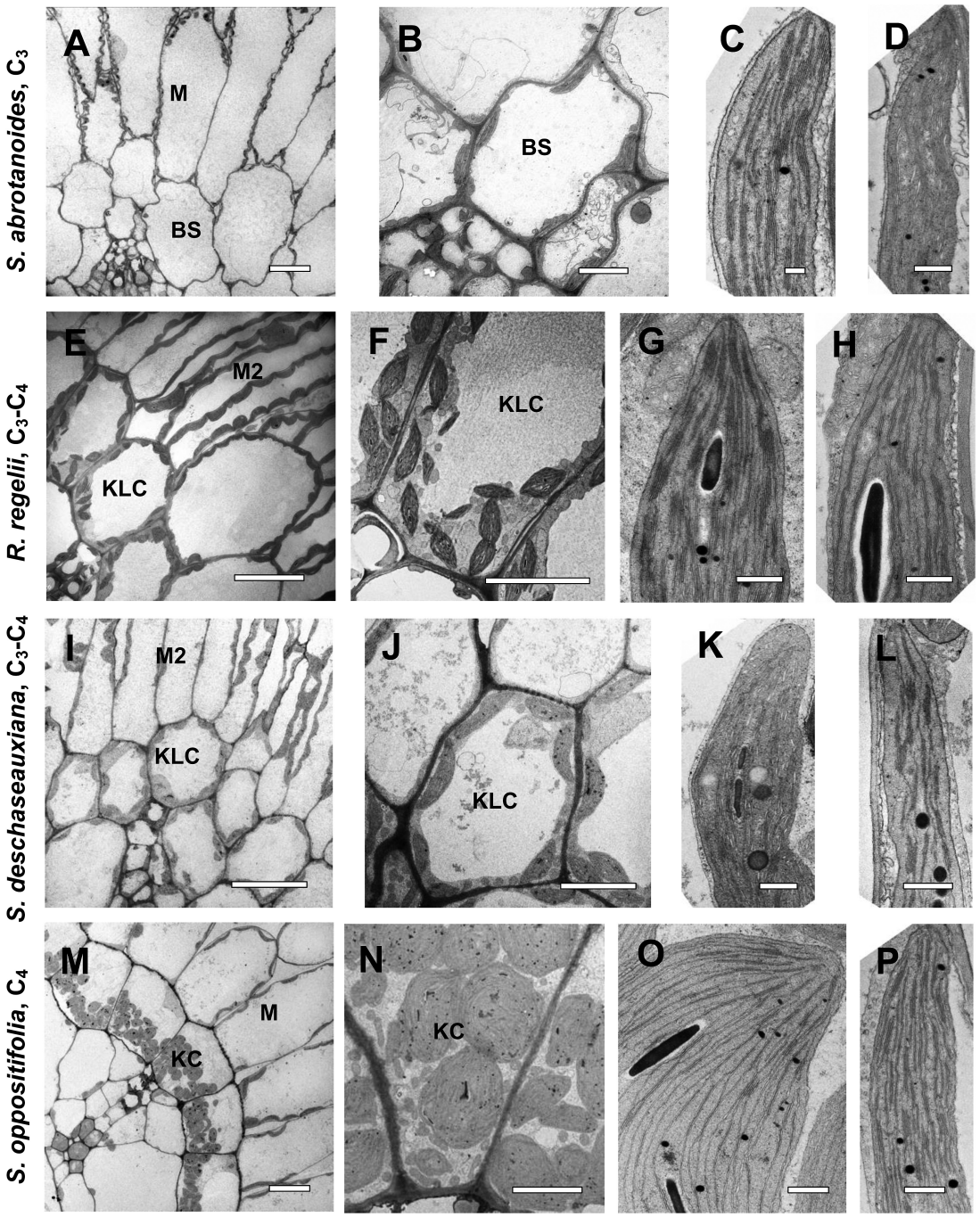

Fig. 3. Electron microscopy of bundle sheath (BS)/Kranz-like cells (KLCs)/Kranz cells (KCs) and mesophyll (M) chlorenchyma cells in leaves of three *Salsola* species and *Rhaphidophyton regelii*: *S. abrotanoides* (A–D), *R. regelii* (E–H), *S. deschaseauxiana* (I–L), and *S. oppositifolia* (M–P). (A, E, I, M) Micrographs show M and BS/KLC/KC around vascular bundles. (B, F, J, N) Organelle distribution in BS/KLC/KC at a higher magnification. Note the difference in abundance of organelles in BS/KLC/KC between species, and the numerous mitochondria in KLCs of *R. regelii* (F) and *S. deschaseauxiana* (J), and in KCs in *S. oppositifolia* (N). (C, G, K, O) Chloroplast structure in BS/KLC/KC. (D, H, L, P) Structure of M chloroplasts. Scale bars = 20 μm for (A, I, M); 10 μm for (E,J, M); 5 μm for (N); 1 μm for (F); 0.5 μm for (B–D, G, H, K, L, O, P).

some mitochondria located in a centrifugal position. The structure of the thylakoid system was similar for BS and M chloroplasts (Fig. 3C, D).

In the KLCs of four species identified as C_3–C_4 intermediates, *R. regelii* (Fig. 3E, F), *S. deschaseauxiana* (Fig. 3I, J), *S. gymnomaschala*, and *S. verticillata* (not shown), the chloroplasts were at least twice as numerous (per cell section) than those of the BS in *S. abrotanoides*; they were distributed along the cell wall but tended to be enriched in the centripetal position. The mitochondria were also twice as numerous (per cell section) and 1.5–2 times larger than in BS cells of *S. abrotanoides*; and most of them were located in the centripetal position, close to the inner periclinal or radial cell walls (Fig. 3F, J). KLC chloroplasts (Fig. 3G, K) and M chloroplasts (Fig. 3H, L) in *R. regelii* and *S. deschaseauxiana* (and the other two *Salsola* intermediates, not shown) had a similar structure with a well-developed system of medium-sized grana consisting of 7–11 thylakoids.

The KCs in C_4 *S. oppositifolia* contained numerous organelles in the centripetal position (Fig. 3M, N). The chloroplast structure differed remarkably among M cells and KCs: while the M chloroplasts had small to medium-sized grana of 2–5 thylakoids in stacks (Fig. 3P), the KC chloroplasts had numerous single thylakoids that interconnect small grana of paired thylakoids, or a few grana consisting mostly of 3–5 thylakoids (Fig. 3O).

Mitochondria in BS and M cells of *S. abrotanoides* had a similar size and structure (~0.4 µm), whereas in the KLCs of *S. deschaseauxiana*, *S. gymnomaschala*, *S. verticillata*, and *R. regelii* they were about 1.3–1.5 times larger compared to the M cells. In KCs and M cells of *S. oppositifolia* the mitochondria were almost identical in size (~0.5 µm).

Carbon isotope composition ($\delta^{13}C$) and CO_2 compensation point (Γ)

Of the species studied biochemically and physiologically here, *S. oppositifolia* had C_4 $\delta^{13}C$ values (–13.7 ‰) while the other species had $\delta^{13}C$ values ranging from –28.8 to –31.5‰, typical for C_3 plants (Table 2).

Γ was measured at 25 °C, 1000 PPFD, and 20% O_2 in mature leaves of six *Salsola* species and *R. regelii* (Table 2). *Γ* values were characteristic of C_4 species for *S. oppositifolia* (3.7 µmol mol^{-1}) and characteristic of C_3 species for *S. abrotanoides* (61.2 µmol mol^{-1}). The *Γ* values in the other five species (*R. regelii*, *S. deschaseauxiana*, *S. gymnomaschala*, *S. verticillata*, and *S. divaricata*) were intermediate between C_3 and C_4, being about 32 µbar in the four *Salsola* species and 36.2 µmol mol^{-1} in *R. regelii* (Table 2).

Immunolocalization of GDC

In situ immunogold labeling for GDC using the antibody to the P protein was examined by electron microscopy, and a quantitative analysis was made based on the density of gold particles, in C_3 *S. abrotanoides*, C_3–C_4 *R. regelii*, *S. deschaseauxiana*, *S. gymnomaschala*, and *S. verticillata*, along with the C_3–C_4 species *S. divaricata* and C_4 *S. oppositifolia*. Analysis of the immunolabeling distribution showed that there was no significant difference in density of the gold particles between the mitochondria of M and BS cells in C_3 *S. abrotanoides* (Fig. 4, Supplementary Fig. S2). In contrast, in the C_4 species *S. oppositifolia* gold particles were selectively localized in KC mitochondria with low labeling in M mitochondria, with a 10-fold difference in their number. In the intermediates *R. regelii*, *S. deschaseauxiana*, *S. gymnomaschala*, and *S. verticillata*, as well as in *S. divaricata*, the number of gold particles was also ~5.8–10 times higher in KLCs compared to M mitochondria (Fig. 4).

Western blot analysis of key C_4 enzymes

Immunoblots for the key C_4 cycle enzymes PEPC, PPDK, NAD-ME, and NADP-ME from total soluble proteins extracted from leaves of the studied species are presented in Fig. 5. The C_4 species *S. oppositifolia* had very high labelling for the C_4 pathway enzymes, PEPC and PPDK, and the two decarboxylases, NADP-ME and NAD-ME. Compared to the C_4 species, the C_3 species *S. abrotanoides* and the C_3–C_4 intermediates *R. regelii*, *S. deschaseauxiana*, *S. gymnomaschala*, *S. verticillata*, and *S. divaricata* had very low labelling for the C_4 cycle enzyme PPDK and, to varying degrees, less labelling for PEPC, NAD-ME, and NADP-ME.

Molecular phylogeny of Salsoleae and mapping of key traits

The molecular phylogenetic analysis of the chloroplast genome revealed two unambiguous C_4 lineages in Salsoleae *s.s.*, (1) *Halothamnus*, and (2) *Anabasis* clade + *Noaea* clade +

Table 2. *Carbon isotope discrimination ($\delta^{13}C$) and CO_2 compensation point (Γ) for a subset of Salsoleae* s.s. *Values with different letters are significantly different according to one-way ANOVA with a* post hoc *Tukey HSD.*

Species	Carbon isotope discrimination $\delta^{13}C$, ‰	CO_2 compensation point, *Γ*, µmol mol^{-1}
S. abrotanoides, C_3	-31.2 ± 0.6 (*n* = 4) a	61.2 ± 0.7 (*n* = 2) a
R. regelii, C_3–C_4	-31.5 ± 0.3 (*n* = 8) a	36.1 ± 2.2 (*n* = 4) b
S. deschaseauxiana, C_3–C_4	-29.9 ± 0.3 (*n* = 6) ab	31.9 ± 1.8 (*n* = 4) b
S. gymnomaschala, C_3–C_4	-28.8 ± 0.3 (*n* = 12) b	31.2 ± 1.0 (*n* = 3) b
S. divaricata, C_3–C_4	-29.9 ± 0.3 (*n* = 16) ab	33.3 ± 2.5 (*n* = 3) b
S. verticillata, C_3–C_4	-29.1 ± 0.4 (*n* = 14) b	32.2 ± 2.0 (*n* = 6) b
S. oppositifolia, C_4	-13.0 ± 0.3 (*n* = 6) c	3.7 ± 0.9 (*n* = 4) c

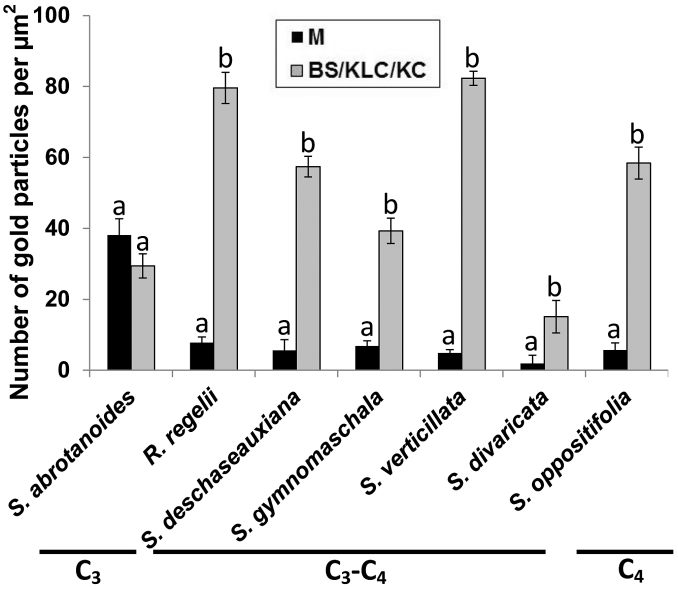

Fig. 4. Quantitative data on GDC immunolabeling in mesophyll (M) and bundle sheath (BS)/Kranz-like cells (KLC)/Kranz cells (KC) for a subset of Salsoleae. The background labeling was low and did not exceed 4.0. Different letters indicate significant differences between M and BS/KLC/KC according to Tukey's HSD (honest significant difference) test.

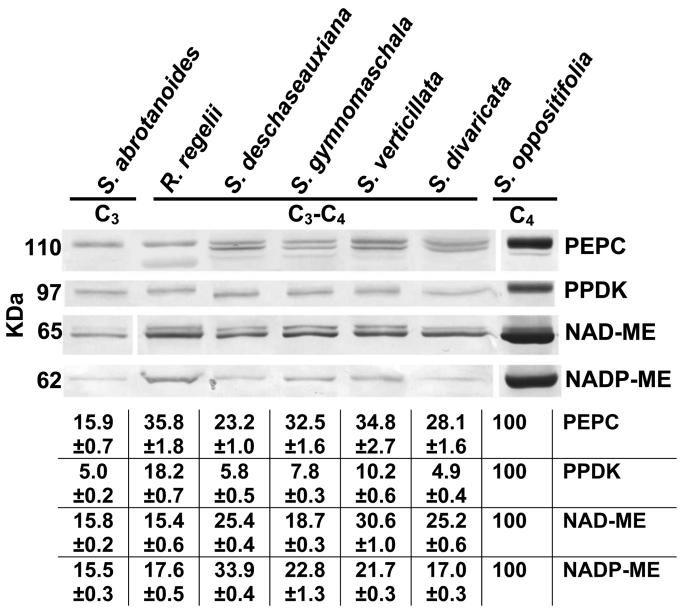

15.9 ±0.7	35.8 ±1.8	23.2 ±1.0	32.5 ±1.6	34.8 ±2.7	28.1 ±1.6	100	PEPC
5.0 ±0.2	18.2 ±0.7	5.8 ±0.5	7.8 ±0.3	10.2 ±0.6	4.9 ±0.4	100	PPDK
15.8 ±0.2	15.4 ±0.6	25.4 ±0.4	18.7 ±0.3	30.6 ±1.0	25.2 ±0.6	100	NAD-ME
15.5 ±0.3	17.6 ±0.5	33.9 ±0.4	22.8 ±1.3	21.7 ±0.3	17.0 ±0.3	100	NADP-ME

Fig. 5. Western blots for C_4 enzymes from soluble proteins extracted from leaves of six *Salsola s.l.* species, *S. abrotanoides*, *S. deschaseauxiana*, *S. gymnomaschala*, *S. verticillata*, *S. divaricata*, *S. oppositifolia*, and *Rhaphidophyton regelii*. Blots were probed with antibodies raised against PEPC, PPDK, NAD-ME, and NADP-ME: representative western blots are presented showing detection of each protein. The originals were modified for alignment according to species; there were no selective changes in the mass or densities of bands on the membrane. The molecular mass is indicated to the left of the blots. The table gives a quantitative representation of the western blot data in percentage terms, where 100% refers to the level found in leaves of C_4 *S. oppositifolia*.

Haloxylon clade. Since the *Anabasis* clade, *Noaea* clade, and *Haloxylon* clade formed a polytomy with two C_3–C_4 intermediate clades, a higher number of three or four C_4 origins is possible (Supplementary Fig. S3). When using a narrower outgroup (only *Salsola genistoides*) the two C_3–C_4 intermediate clades merged into a monophyletic group that still formed a polytomy with the *Anabasis* clade, *Noaea* clade, and *Haloxylon* clade (Fig. 6). From the crown group age of *Halothamnus* (7.9–1.3 mya), *Anabasis* (10.2–2.6 mya), and *Noaea* (10.3–2.8 mya) it can be assumed that in these lineages C_4 photosynthesis has been present since the Late Miocene/Early Pliocene. Only for the *Haloxylon* clade can a distinctly older minimum age for the origin of C_4 photosynthesis of 16.9–6.6 mya be inferred from the molecular dating. In the case of common ancestry of the *Anabasis* clade + *Noaea* clade + *Haloxylon* clade, C_4 photosynthesis might date back to 19.2–7.6 mya (Supplementary Fig. S3).

The ML character optimization inferred a perennial life form and fully developed leaves without massive central sclerenchyma as the ancestral condition in Salsoleae *s.s.* (Fig. 6). An annual life form evolved at least six times independently in the tribe. A massive central sclerenchyma also evolved repeatedly (Fig. 6). In some cases, this feature was characteristic at the generic level, as in *Girgensohnia*, *Horaninovia*, *Cornulaca*, *Raphidophyton*, and *Noaea*. The reduction or complete loss of a true leaf lamina and a shift of photosynthetic function to the young stems was a common feature in Salsoleae and evolved multiple times in C_4 lineages of Salsoleae *s.s.*, but also in *S. genistoides*. The occurrence of leafless species was clustered in certain genera, such as *Anabasis*, *Haloxylon*, and *Hammada*, the latter of which seemed to be highly polyphyletic.

Furthermore, the ML character optimization inferred a C_3 metabolism and C_3-type BS cells as ancestral in Salsoleae *s.s.* According to the ancestral character state reconstruction, a switch towards C_4 seems to have already occurred along the branch leading to the large sister group of the C_3 species *Salsola pachyphylla*, which contains three C_4 subclades but also one clade of C_3 and C_3–C_4 intermediates (highlighted green in Fig. 6). This clade of C_3 and C_3–C_4 intermediate species did not contain any C_4 species, and the clade was part of a polytomy of C_4 clades; thus, there is no indication in the cp tree that the C_3–C_4 intermediates represent ancestral states leading towards full C_4 photosynthesis.

Resolution in the ITS tree was weak in many parts of the tree (Supplementary Fig. S4). Combining cp and ITS data resulted in very low resolution (tree not shown) due to conflicting topologies. Branches that were in conflict between the two data sets (with bootstrap >75) are marked on the ITS tree (Supplementary Fig. S4).

Discussion

Evidence for newly identified C_3–C_4 species in Salsoleae

Results from gas exchange (Γ), compartmentation of GDC between M cells and KLCs, analyses of carbon isotope composition, and analyses of levels of C_4 enzymes, along with the structure of the respective cells, indicated that four species, *S. deschaseauxiana*, *S. gymnomaschala*, *S. verticillata*, and *R. regelii*, are C_3–C_4 intermediates, while

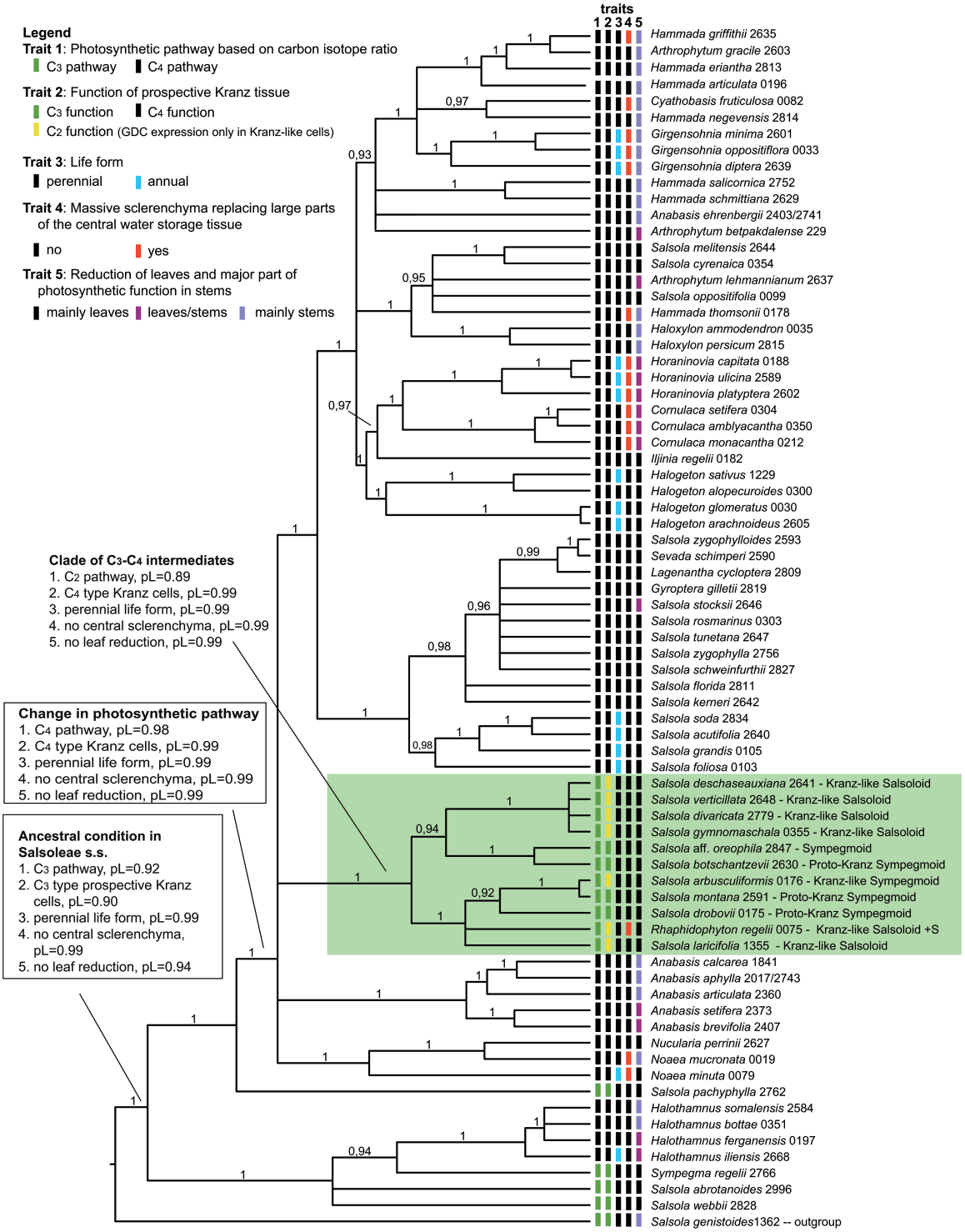

Fig. 6. Molecular phylogenetic tree of Salsoleae *s.s.* (Chenopodiaceae) based on four cp markers (*atpB-rbcL* spacer, *ndhF-rpl32* spacer, *trnQ-rps16* spacer, *rpl16* intron) and 74 representative species. The tree was calculated using the program package BEAST (posterior probabilities are shown above branches) and was rooted with *Salsola genistoides*. Character optimization was conducted using Mesquite and ancestral conditions are indicated for selected nodes (pL = proportional likelihood).

S. abrotanoides operates C_3 photosynthesis. Analyses of the carbon isotope composition of these four intermediates as well as the C_3–C_4 intermediate *S. divaricata* showed they all have values in the range of those of C_3 species compared to the C_4-type value in *S. oppositifolia* (Table 2). However, values for plants grown in growth chambers are more negative (i.e. up to 4–7‰) than samples from natural habitats (Voznesenskaya *et al.*, 2013). The more positive $\delta^{13}C$ values in the natural habitat may be due to growth under arid conditions limiting CO_2 diffusion into leaves (Cerling, 1999), or to induction of a partially functional C_4 cycle. According to our study, among Salsoleae there are at least 19 species with C_3 isotope values, seven of which are C_3–C_4 species (Table 1).

Structural, biochemical, and functional analyses are needed in order to determine whether species having C_3-type $\delta^{13}C$ values are C_3, proto-Kranz, or C_3–C_4. An important test is measurement of Γ, since values are lower in C_3–C_4 than in C_3 plants, which is indicative of a reduction in photorespiration (Edwards and Ku, 1987). Gas exchange analyses of *S. deschaseauxiana*, *S. gymnomaschala*, *S. verticillata*, and *R. regelii* showed that all these species have Γ values that are intermediate between C_4 *S. oppositifolia* and C_3 *S. abrotanoides* (Table 2). Additionally, C_3–C_4 intermediates, like C_4 species, have selective compartmentation of GDC in KLC mitochondria (Rawsthorne *et al.*, 1988; Voznesenskaya *et al.*, 2001, 2013; Sage *et al.*, 2012, 2014), supporting refixation of photorespired CO_2. Analysis of GDC levels by immunolocalization in these four intermediates indicated selective localization in mitochondria of Kranz-like cells (KLCs), while in the C_3 species *S. abrotanoides* the density of immunolabeling for GDC was similar in M and BS mitochondria.

Western blot analysis of C_4 enzymes showed that levels in the C_3 species *S. abrotanoides* and the C_3–C_4 intermediates *S. deschaseauxiana*, *S. gymnomaschala*, *S. verticillata*, and *R. regelii* were very low compared to the C_4 species *S. oppositifolia*. The levels of PEPC in the four C_3–C_4 intermediate species were higher than in the C_3 species *S. abrotanoides*. However, except for *R. regelii*, levels of PPDK were low and barely detectable in both the C_3 and intermediate species. *R. regelii* had higher levels of PPDK, but low levels of C_4 decarboxylases similar to the C_3 species.

Currrently, the results suggest that all seven known C_3–C_4 species of Salsoleae, *R. regelii*, *S. arbusculiformis*, *S. deschaseauxiana*, *S. divaricata*, *S. gymnomaschala*, *S. laricifolia*, and *S. verticillata* (Voznesenskaya *et al.*, 2001, 2013; Wen and Zhang, 2015; this study, Table 1), are Type I, where the reduction of Γ comes from refixation of photorespired CO_2 in KLCs with little or no function of a C_4 cycle (Edwards and Ku, 1987). Whether there is a contribution from a limited C_4 cycle to photosynthesis in these intermediates could be more directly analyzed by the method of Alonso-Cantabrana and von Caemmerer (2016) via online measurements of photosynthesis and carbon isotope discrimination.

A model for evolution of C_4 photosynthesis in Salsoleae based on identified photosynthetic phenotypes

Of the 77 species of Salsoleae analyzed, without those of the *Kali* clade (Table 1), 24 species were studied for the first time. Our sampling was comprehensive and surpasses Carolin *et al.* (1975) with 43 species and Pyankov *et al.* (2001) with 38 species. Of the 77 species, 19 had C_3-type carbon isotope composition (consisting of seven C_3 species, five proposed proto-Kranz species, and seven C_3–C_4 intermediates) while 58 were C_4 species with C_4-type carbon isotope composition and Salsoloid-type leaf anatomy (Table 1). In Fig. 7 five photosynthetic phenotypes in Salsoleae are described based on the anatomical, ultrastructural, and biochemical analyses of species in the current study together with a few species described by Voznesenskaya *et al.* (2013). In this model, C_4 is proposed to have evolved structurally and functionally from C_3 Sympegmoid to Proto-Kranz Sympegmoid to C_3–C_4 Kranz-like Sympegmoid to C_3–C_4 Kranz-like Salsoloid to C_4 Salsoloid-type anatomy. There are two subtypes of Kranz-like Salsoloid C_3–C_4 intermediates (with or without sclerenchyma) and five anatomical subtypes with Salsoloid type.

Non-Kranz anatomy, functionally C_3

The Sympegmoid leaf type is anatomically and functionally C_3. It is characterized by usually two well-developed layers of palisade M cells (M1 and M2) and indistinct C_3-type BS cells around peripheral VBs containing only a few organelles. Species of this type have C_3 $\delta^{13}C$ values, C_3-type Γ values, and structural features of M and BS cells characteristic of C_3 plants (including the occurrence of GDC in both M and BS mitochondria). It is found in *S. abrotanoides* (this study, Figs. 1A, 3, 4), *S. genistoides*, *S. oreophila*, *S. pachyphylla*, *S. webbii* (Carolin *et al.*, 1975; Voznesenskaya, 1976; P'yankov *et al.*, 1997; Pyankov *et al.*, 2001; Voznesenskaya *et al.*, 2013), and *Sympegma regelii* (Wen and Zhang, 2011). Based on anatomical evidence alone, we conclude that *Salsola tianschanica*. belongs to this group, which would then comprise seven species in total (Table 1). An additional trait observed in this group is the comparatively low volume of water storage (WS) tissue and the position of peripheral VBs embedded in the WS tissue rather than at its periphery (Fig. 1A). From known data and the taxonomic literature, in particular the pertinent revisions of section *Coccosalsola* by Botschantzev (1976, 1989), the occurrence of this leaf type in other species is unlikely.

Proto-Kranz anatomy, functionally C_3

Proto-Kranz species have anatomical changes in BS cells that may be the earliest phase of C_4 evolution, preceding development of the C_2 cycle (Sage *et al.*, 2014). In Salsoleae, the Proto-Kranz Sympegmoid type only differs from the Sympegmoid type by having distinct cells with chloroplasts and mitochondria arranged preferentially along the inner and the radial walls between peripheral VBs and the chlorenchyma (Fig. 7). Currently this type is only documented in *S. montana* (Voznesenskaya *et al.*, 2013). It has C_3-like $\delta^{13}C$ and Γ values, and immunolabeling for GDC is similar for M and BS mitochondria. However, based on analysis of leaf anatomy (by light microscopy of fresh leaf or herbarium samples fixed in FAA) there are additional probable candidates for proto-Kranz anatomy among the Central Asian *Salsola* species that have C_3 $\delta^{13}C$ values, namely *S. botschantzevii*, *S. drobovii*, *S. junatovii*, and *S. lipschitzii* (Table 1).

Kranz-like anatomy, functionally C_3–C_4 intermediate

Anatomically there are two types of intermediates in Salsoleae, the Kranz-like Sympegmoid type, and the Kranz-like Salsoloid type (Fig. 7). They resemble C_4 *Salsola* species in having KLCs with numerous organelles in the centripetal position. Both have C_3-type $\delta^{13}C$ values, selective localization of GDC in KLC mitochondria, and intermediate Γ values indicating functionally C_2-type species.

The Kranz-like Sympegmoid type is very similar to the aforementioned Sympegmoid forms; but the outer M cells

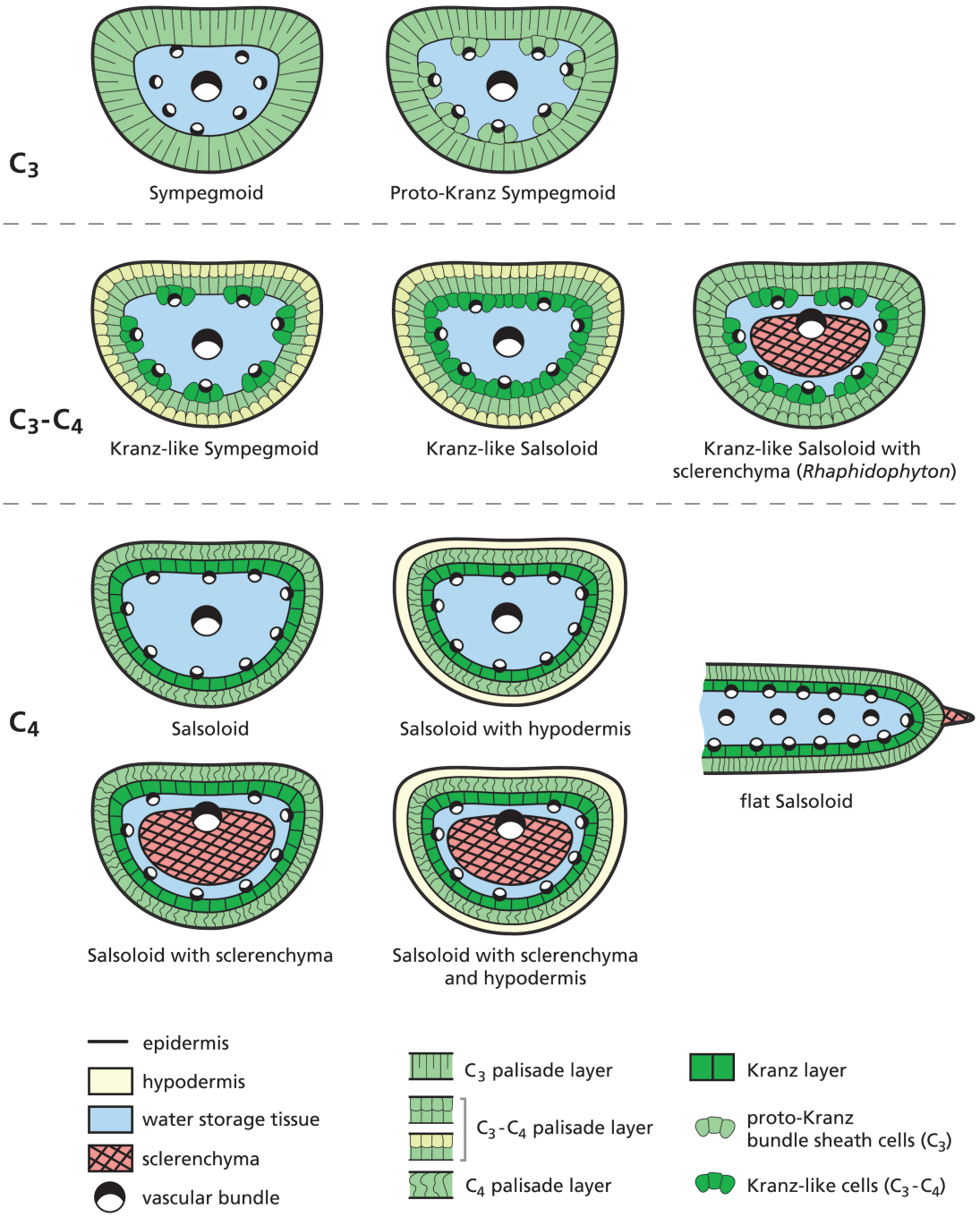

Fig. 7. Anatomical schemes of leaf types found in Salsoleae *s.s.*

(M1) are distinctly shorter and smaller than the inner M cells (M2) and the KLCs are restricted to the peripheral VBs. This type of structure has so far only been found in *S. arbusculiformis* (Voznesenskaya *et al.*, 2001), and it is suggested to represent the first functional step towards C_4-type anatomy.

In the Kranz-like Salsoloid type of intermediacy, the M1 appear more like the hypodermal cells in C_4 species, while still containing more or less numerous chloroplasts. M1 cell size and M/KLC ratio is reduced in comparison with the Sympegmoid types, and the KLCs form a more or less continuous layer (interrupted by crystal-containing idioblasts) around the leaf, as in C_4 *Salsola* species. The KLCs contain chloroplasts and numerous large mitochondria positioned towards the inner cell wall, characteristic of other C_3–C_4 intermediate species (Edwards and Ku, 1987; Rawsthorne and Bauwe, 1998; Voznesenskaya *et al.*, 2007, 2010; Muhaidat *et al.*, 2011; Sage *et al.*, 2012, 2014). This type is currently found in six species (Table 1): *S. laricifolia* (Wen and Zhang, 2011, 2015), *S. divaricata* (Voznesenskaya *et al.*, 2013), and *S. deschaseauxiana*, *S. gymnomaschala*, *S. verticillata*, and *R. regelii* (this study, Figs 1 and 7). However, *R. regelii* represents a different subtype by its very strong central sclerenchyma (Fig. 2), which, according to our knowledge, is unique among the C_3–C_4 intermediates identified in Salsoloideae.

Of note in the Kranz-like Salsoloid type, considerable variation occurs, mainly in the size, shape and the number of

organelles in the M1 cell layer and the arrangement of the KLCs. Sometimes multiple sections within species revealed a certain degree of variation, showing phenotypes more similar to the Kranz-like Sympegmoid type or phenotypes approaching C_4 plants with typical Salsoloid leaf anatomy. Therefore, more detailed studies are needed to assess the phenotypic plasticity of the functionally intermediate types.

Kranz-type anatomy, functionally C_4

The Salsoloid leaf anatomy in C_4 lineages of Salsoleae differs substantially from C_4 eudicots having Atriplicoid-type leaf anatomy with Kranz anatomy around individual veins in flat leaves. Species with Salsoloid-type anatomy are functionally C_4, with a continuous layer of Kranz cells (KC) around WS tissue and VBs. If the M1 layer of cells is present it occurs as a hypodermis with few or no organelles. There is a further reduction in the M/KC ratio, with organelles in the KCs in a centripetal (or, rarely, in centrifugal) position. In other lineages, as in *Halothamnus*, *Noaea*, *Kali*, *Nanophyton*, and *Climacoptera*, the hypodermis is lacking (Kadereit *et al.*, 2003; Wen and Zhang, 2011). Our data on *S. oppositifolia*, and on several other C_4 species that had not previously been studied, do not add substantially to the well-known Salsoloid-type anatomy. Together with 40 other species, *S. oppositifolia* displayed the most common Salsoloid type that has a hypodermis and lacks central sclerenchyma; on the other hand only 12 species account for the variant with central sclerenchyma. The Salsoloid type without a hypodermis and without central sclerenchyma was represented in our sampling by four species of *Halothamnus* only. This form is present in many other species of that genus (Kothe-Heinrich, 1993), and in almost all species of *Kali* (Rilke, 1999), while the variant with a central sclerenchyma was seen only in the two *Noaea* species.

Comparison with the 'Flaveria model' for C_4 evolution

The various photosynthetic phenotypes in Salsoleae fit the general model of evolution from C_3 to proto-Kranz, to intermediates, to Kranz anatomy with a progressive reduction in functional losses due to photorespiration. However, in the '*Flaveria* model' where Kranz anatomy forms around individual veins (Edwards and Ku, 1987; Sage *et al.*, 2012) the structural modifications are very different from the modifications from a Sympegmoid type to a Salsoloid Kranz type where the Kranz anatomy is formed around all veins and WS tissue. In evolution from C_3 to C_4 with Kranz anatomy around individual veins, there is increased vein density and size of BS cells around veins as they develop KC features. In contrast, in the Salsoleae the vein density in C_4 species does not appear to be higher than in the C_3 species. In addition, the size of the KCs is not significantly increased in the C_4 species in comparison with their forerunners in C_3 species (Voznesenskaya *et al.*, 2013). Furthermore, in the Salsoleae model (see fig. 9 in Voznesenskaya *et al.*, 2013) a decrease in the M/KC ratio might also be a precondition, as in grasses (Christin *et al.*, 2013) and dicots (Sage *et al.*, 2012); however, it happens by development of a continuous layer of KCs and reduction in the M1 layer rather than by an increase of veins and BS size.

Where and when did C_4 photosynthesis originate in Salsoleae?

The chloroplast gene tree of Salsoloideae resolves five primary clades in the subfamily, namely the *Nanophyton* clade, the Caroxyloneae clade, the *Salsola genistoides* clade, the *Kali* clade, and the Salsoleae *s.s.* clade (Supplementary Fig. S3; Kadereit and Freitag, 2011), with the first four forming the sister group to Salsoleae *s.s.* (Supplementary Fig. S3). Molecular trees based on the nrDNA marker ITS (Supplementary Fig. S4) also reveal these clades but they are contradictory in their positions (for a short discussion on this matter see Supplemetary Fig. S3). According to our results in both data sets only two clearly independent C_4 lineages in Salsoleae seem likely. The first lineage is *Halothamnus*, with a crown age of 7.9–1.3 mya, and probably plus the *Kali* clade in the ITS data set. Most species of both clades have Salsoloid leaf anatomy and lack a hypodermis (e.g. as in *Traganum*). In the cp tree the monospecific C_3 genus *Sympegma* is sister to *Halothamnus* while in the ITS tree it is sister to all C_3–C_4 intermediates and C_4 clades in the Salsoleae *sensu lato* (*s.l.*, Supplementary Fig. S4). The *Halothamnus* and *Kali* clades seem to have no close relatives with a C_3–C_4 intermediate phenotype. The second C_4 lineage in Salsoleae *s.s.* probably consists of all other C_4 species. Since the C_4 clades of *Anabasis*, *Noaea*, and *Haloxylon* form a polytomy with the C_3–C_4 intermediates clade in the cp tree (Fig. 6), one large monophyletic C_4 clade and a sister-group relationship to the C_3–C_4 intermediates remains possible. Unfortunately, the weak resolution of this particular part of the ITS tree within Salsoleae *s.s.* does not support this (Supplementary Fig. S4). The overall similar Salsoloid leaf anatomy with hypodermis (except for the two species of *Noaea*) and NADP-ME biochemistry is in favor of common ancestry of the C_4 syndrome in this lineage. The predicted age of this large C_4 lineage in Salsoleae *s.s.* is 19.2–7.6 mya (Supplementary Fig. S3), which is in accordance with the origin of many other C_4 lineages during the Middle to Late Miocene (Christin *et al.*, 2011).

Does the C_3–C_4 intermediate condition represent an ancestral state to C_4 in Salsoleae? Is there phylogenetic evidence for a reversion from C_4 back to C_3?

The ML optimization suggests that early Salsoleae were shrubs or subshrubs that performed C_3 photosynthesis in well-developed leaves with a Sympegmoid leaf type (Fig. 6). Along with one C_3 species (*S. oreophila*), 10 species (consisting of proto-Kranz and C_3–C_4 intermediates) in Salsoleae form one (Fig. 6) or two clades (Supplementary Fig. S3) in the cp trees. Lack of resolution in the phylogenetic trees just at the node where these phenotypes and their closest C_4 relatives arise hampers a reconstruction of these proto-Kranz and C_3–C_4 intermediates as ancestral (see also Supplementary Fig. S4). The ML optimization even suggests that the node from which these phenotypes arise was most likely C_4 (pL=0.98, Fig. 6), which would imply the origin of these C_3–C_4 species from C_4. However, in general a reversion from C_4 back to C_3 or intermediate phenotypes seems to be exceedingly rare, if

not improbable. Although a few cases have been reported in which C_3 species or C_3–C_4 intermediates are nested in a C_4 clade, there has also been plausible evidence for a scenario of multiple C_4 origins (e.g. Ocampo *et al.*, 2013; Bohley *et al.* 2015). In the case of Salsoleae *s.s.*, we assume that a convincing reconstruction is severely hampered by the low number of C_3–C_4 intermediate lineages (not by the low number of intermediate species) since all C_3–C_4 intermediate species seem to belong to just one lineage.

This C_3–C_4 intermediate-rich lineage might, however, be of major interest for future studies. Studying the ecology, physiology, and biochemistry of closely related proto-Kranz and C_3–C_4 intermediate species with and without selective localization of GDC might provide further insights into the selective advantage of proto-Kranz anatomy and the C_2 pathway. So far the selective advantage of displacement of BS organelles towards the centripetal position in proto-Kranz compared to C_3 species is not clear. Possibly the proto-Kranz state leads to a slight increase in refixation of the CO_2 generated by GDC in BS cells; however, this could be difficult to detect experimentally (e.g. by measurements of Γ). A C_2 cycle is indeed able to generate distinctly higher CO_2 levels in leaves (Keerberg *et al.*, 2014) and therefore has an ecophysiological advantage. Since a reversion from intermediate to C_3 still seems possible in this clade (*S. oreophila*), there is a need for further sampling and deeper resolution within this lineage.

Reduction of leaf lamina combined with photosynthesis being taken over by the green stem cortex evolved multiple times in Salsoleae; however, except for *S. genistoides*, this is only observed in the C_4 clades. We hypothesize that the higher productivity of the C_4 cycle in Salsoleae allows for a reduction in the surface area and the amount of photosynthetic tissue, reduction of transpiration, and an increase in water use efficiency. This is obviously advantageous in the extremely dry habitats of the Eurasian deserts and semi-deserts that the Salsoleae have successfully colonized.

Conclusions

In the model for evolution of C_4 in Salsoleae, putative C_3 ancestors have M tissue surrounding the entity of veins with a limited volume of WS tissue; differentiation occurs with development of KLCs next to minor veins, reduction in size of M cells, and ultimately development of an internal layer of KLCs that surrounds all the vascular and WS tissue. Compared to the '*Flaveria* model' for C_4 development around individual veins, in Salsoleae the proposed biochemical and functional transitions suggest convergence; however, there is obvious divergence in how structural changes were made in C_3 ancestors to develop Kranz anatomy. In Salsoleae, a number of structural changes that are important in the evolution of C_4 flat-leaved species are missing: individual KC size often does not increase, but KC volume increases due to the formation of the continuous layer, a decrease of the M/KC ratio occurs mainly due to the reduction of the M1 layer, and the density of venation does not change. These differences might be related to the succulent nature of Salsoleae, with an increase of the volume of WS tissue during the transition from C_3 to C_3–C_4 intermediates and to C_4 species.

The Salsoleae phylogenies unambiguously reveal all C_3 species, except for *S. oreophila*, in basal positions, and both the C_4 species and the C_3–C_4 intermediates as derived, but occurring in different clades. Intermediates, proto-Kranz, and one C_3 species are clustered in one (cp tree) or four (ITS tree) monophyletic groups that might either be sister to a large C_4 clade or nested within it. In the absence of closely related C_4 species, their intermediacy cannot be determined as ancestral; although they display logical stepwise, 'model-conforming' phenotypes from C_3 to C_4 photosynthesis. From a phylogenetic point of view, they may represent an evolutionarily independent solution, enabling the respective species to survive in harsh environments, even in competition with distantly related species of the same tribe possessing full C_4 photosynthesis.

Supplementary data

Supplementary data are available at *JXB* online

Table S1. Details of the specimens of Salsoleae and outgroups included in the molecular analyses.

Table S2. Sampling of primary clades of Salsoloideae (Salsoleae, Caroxyloneae, *Nanophyton* clade, *Salsola kali* clade and *Salsola genistoides* clade).

Table S3. Primers, PCR recipes and cycler programs.

Fig. S1. Representative membrane stained with Ponceau S after transfer of proteins to a nitrocellulose membrane and before immunoblotting.

Fig. S2. Electron microscopy of *in situ* immunolocalization of GDC in chlorenchyma cells of *Salsola abrotanoides* (C_3),*Rhaphidophyton regelii* (C_3–C_4), *S. verticillata* (C_3–C_4), and *S. oppositifolia* (C_4).

Fig. S3. Dated molecular phylogenetic tree of Salsoloideae (Chenopodiaceae) based on four cp markers (*atpB-rbcL* spacer, *ndhF-rpl32* spacer, *trnQ-rps16* spacer, *rpl16* intron).

Fig. S4: ML tree based on ITS sequences of Salsoleae and Caroxyloneae with representatives of Salicornioideae and Suaedoideae as the outgroup.

Acknowledgements

This work was supported by the National Science Foundation under funds MCB #1146928 to GEE, EV, NK; partly by the Russian Foundation of Basic Research under grants 12-04-00721 and 15-04-03665 for EV, NK; and by the German Science Foundation (DFG; grant KA1816/7-1 to GK). We are grateful to the Core Facility Center 'Cell and Molecular Technologies in Plant Science' of Komarov Botanical Institute (St Petersburg, Russia) and Franceschi Microscopy and Imaging Center of Washington State University for use of their facilities and staff assistance, and to C. Cody for plant growth management. We thank D. Franke (Mainz) for help with the illustrations and C. Wild (Mainz) for curating the chenopod living collection at Mainz Botanical Garden.

References

Akhani H, Edwards G, Roalson EH. 2007. Diversification of the Old World Salsoleae *s.l.* (Chenopodiaceae): Molecular phylogenetic analysis of nuclear and chloroplast data sets and a revised classification. International Journal of Plant Sciences **168,** 931–956.

Akhani H, Ghasemkhani M. 2007. Diversity of photosynthetic organs in Chenopodiaceae from Golestan National Park (NE Iran) based on carbon isotope composition and anatomy of leaves and cotyledons. Nova Hedwigia Beiheft **131,** 265–277.

Akhani H, Trimborn P, Ziegler H. 1997. Photosynthetic pathways in Chenopodiaceae from Africa, Asia and Europe with their ecological, phytogeographical and taxonomical importance. Plant Systematics and Evolution **206,** 187–221.

Alonso-Cantabrana H, von Caemmerer S. 2016. Carbon isotope discrimination as a diagnostic tool for C_4 photosynthesis in C_3–C_4 intermediate species. Journal of Experimental Botany **67,** 3109–3121.

Bender MM, Rouhani I, Vines HM, Black Jr, CC. 1973. $^{13}C/^{12}C$ ratio changes in Crassulacean Acid Metabolism plants. Plant Physiology **52,** 427–430.

Bohley K, Joos O, Hartmann H, Sage R, Liede-Schumann S, Kadereit G. 2015. Phylogeny of Sesuvioideae (Aizoaceae) – Biogeography, leaf anatomy and the evolution of C_4 photosynthesis. Perspectives in Plant Ecology, Evolution and Systematics **17,** 116–130.

Bokhari MH, Wendelbo P. 1978. On anatomy, adaptions to xerophytism and taxonomy of *Anabasis* inclusive *Esfandiaria* (Chenopodiaceae). Botaniska Notiser **131,** 279–292.

Botschantzev VP. 1976. Conspectus specierum sectionis Coccosalsola Fenzl generis *Salsola* L. Novosti Sistematiki Vysshikh rastenii, **13,** 74–102 [in Russian].

Botschantzev VP. 1989. De genere *Darniella* Maire et Weiller et relationes ejus ad genus *Salsola* L. (Chenopodiaceae). Novosti Sistematiki Vysshikh Rastenii **26,** 79–90 [In Russian].

Brown WV. 1975. Variations in anatomy, associations, and origin of Kranz tissue. American Journal of Botany **62,** 395–402.

Carolin R, Jacobs S, Vesk M. 1975. Leaf structure in Chenopodiaceae. Botanische Jahrbücher für Systematik, Pflanzengeschichte und Pflanzengeographie **95,** 226–255.

Cerling TE. 1999. Paleorecords of C_4 plants and ecosystems. In: Sage RF, Monson RK, eds. *C_4 plant biology.* New York: Academic Press, 445–469.

Christin PA, Osborne CP, Sage RF, Arakaki M, Edwards EJ. 2011. C_4 eudicots are not younger than C_4 monocots. Journal of Experimental Botany **62,** 3171–3181.

Christin PA, Osborne CP, Chatelet DS, Columbus JT, Besnard G, Hodkinson TR, Garrison LM, Vorontsova MS, Edwards EJ. 2013. Anatomical enablers and the evolution of C_4 photosynthesis in grasses. Proceedings of the National Academy of Sciences, USA **110,** 1381–1386.

Drummond AJ, Ho SYW., Phillips MJ., Rambaut A. 2006. Relaxed phylogenetics and dating with confidence. PLOS Biology **4,** e88.

Drummond AJ, Rambaut A. 2007. BEAST: Bayesian evolutionary analysis by sampling trees. BMC Evolutionary Biology **7,** 214.

Edwards GE, Ku MS. 1987. Biochemistry of C_3–C_4 intermediates. The Biochemistry of Plants **10,** 275–325.

Edwards GE, Voznesenskaya EV. 2011. C_4 photosynthesis: Kranz forms and single-cell C_4 in terrestrial plants. In: **Raghavendra** AS, Sage RF, eds. C_4 photosynthesis and related CO_2 concentrating mechanisms. Dordrecht: Springer, 29–61.

Fisher AE, McDade LA, Kiel CA, Khoshravesh R, Johnson MA, Stata M, Sage TL, Sage RF. 2015. Evolutionary history of *Blepharis* (Acanthaceae) and the origin of C_4 photosynthesis in section *Acanthodium*. International Journal of Plant Sciences **176,** 770–790.

Freitag H, Duman H. 2000. An unexpected new taxon of *Salsola* from Turkey. Edinburgh Journal of Botany **57,** 339–348.

Freitag H, Stichler W. 2000. A remarkable new leaf type with unusual photosynthetic tissue in a Central Asiatic genus of Chenopodiaceae. Plant Biology **2,** 154–160.

Freitag H, Vural M, Adigüzel N. 1999. A remarkable new *Salsola* and some new records of Chenopodiaceae from Central Anatolia, Turkey. Willdenowia **29,** 123–139.

Gowik U, Westhoff P. 2011. The path from C_3 to C_4 photosynthesis. Plant Physiology **155,** 56–63.

Hancock L, Edwards EJ. 2014. Phylogeny and the inference of evolutionary trajectories. Journal of Experimental Botany **65,** 3491–3498.

Hibberd JM, Covshoff S. 2010. The regulation of gene expression required for C_4 photosynthesis. Annual Review of Plant Biology **61,** 181–207.

Kadereit G, Ackerly D, Pirie MD. 2012. A broader model for C_4 photosynthesis evolution in plants inferred from the goosefoot family (Chenopodiaceae *s.s.*). Proceedings of the Royal Society of London B: Biological Sciences **279,** 3304–3311.

Kadereit G, Borsch T, Weising K, Freitag H. 2003. Phylogeny of Amaranthaceae and Chenopodiaceae and the evolution of C_4 photosynthesis. International Journal of Plant Sciences **164,** 959–986.

Kadereit G, Freitag H. 2011. Molecular phylogeny of Camphorosmeae (Camphorosmoideae, Chenopodiaceae): implications for biogeography, evolution of C_4-photosynthesis and taxonomy. Taxon **60,** 51–78.

Kadereit G, Lauterbach M, Pirie MD, Arafeh R, Freitag H. 2014. When do different C_4 leaf anatomies indicate independent C_4 origins? Parallel evolution of C_4 leaf types in Camphorosmeae (Chenopodiaceae). Journal of Experimental Botany **65,** 3499–3511.

Keerberg O, Pärnik T, Ivanova H, Bassüner B, Bauwe H. 2014. C_2 photosynthesis generates about 3-fold elevated leaf CO_2 levels in the C_3–C_4 intermediate species *Flaveria pubescens.* Journal of Experimental Botany **65,** 3649–3656.

Khatib A. 1959. *Contribution à l'étude systématique anatomique, phylogénetique et écologique des Chénopodiacées de la Syrie*, Thésis Montpellier, Damascus: Imprimérie de l'Université de Damas.

Khoshravesh R, Hossein A, Sage TL, Nordenstam B, Sage RF. 2012. Phylogeny and photosynthetic pathway distribution in *Anticharis* Endl. (Scrophulariaceae). Journal of Experimental Botany **63,** 5645–5658.

Khoshravesh R, Stinson CR, Stata M, Busch FA, Sage RF, Ludwig M, Sage TL. 2016. C_3–C_4 intermediacy in grasses: organelle enrichment and distribution, glycine decarboxylase expression, and the rise of C_2 photosynthesis. Journal of Experimental Botany **67,** 3065–3078.

Kothe-Heinrich G. 1993. Revision der Gattung *Halothamnus* (Chenopodiaceae). Bibliotheca Botanica **143,** 1–176.

Ku MS, Monson RK, Littlejohn RO, Nakamoto H, Fisher DB, Edwards GE. 1983. Photosynthetic characteristics of C_3–C_4 intermediate *Flaveria* species: I. Leaf anatomy, photosynthetic responses to O_2 and CO_2, and activities of key enzymes in the C_3 and C_4 pathways. Plant Physiology **71,** 944–948.

Ku MS, Wu J, Dai Z, Scott RA, Chu C, Edwards GE. 1991. Photosynthetic and photorespiratory characteristics of *Flaveria* species. Plant Physiology **96,** 518–528.

Long JJ, Berry JO. 1996. Tissue-specific and light-mediated expression of the C_4 photosynthetic NAD-dependent malic enzyme of *Amaranth* mitochondria. Plant Physiology **112,** 473–482.

Lyu M-JA, Gowik U, Kelly S, Covshoff S, Mallmann J, Westhoff P, Hibberd JM, Stata M, Sage RF, Lu H. 2015. RNA-Seq based phylogeny recapitulates previous phylogeny of the genus *Flaveria* (Asteraceae) with some modifications. BMC Evolutionary Biology **15,** 1.

Maire R. 1962. *Flore de l'Afrique du Nord.* Vol. **8**. Paris: Paul Lechevalier.

Maurino VG, Drincovich MF, Andreo CS. 1996. NADP-malic enzyme isoforms in maize leaves. Biochemistry and Molecular Biology International **38,** 239–250.

McKown AD, Moncalvo JM, Dengler NG. 2005. Phylogeny of *Flaveria* (Asteraceae) and inference of C_4 photosynthesis evolution. American Journal of Botany **92,** 1911–1928.

Monson RK, Edwards GE, Ku MS. 1984. C_3–C_4 intermediate photosynthesis in plants. Bioscience **34,** 563–574.

Monteil P. 1906. *Anatomie comparée de la feuille des Chénopodiacées.* Thesis Paris, Lons-le-Saunier: Lucien Declumb.

Moore BD, Ku MSB, Edwards GE. 1987. C_4 photosynthesis and light-dependent accumulation of inorganic carbon in leaves of C_3–C_4 and C_4 *Flaveria* species. Australian Journal of Plant Physiology **14,** 657–658.

Muhaidat R, Sage TL, Frohlich MW, Dengler NG, Sage RF. 2011. Characterization of C_3–C_4 intermediate species in the genus *Heliotropium* L. (Boraginaceae): anatomy, ultrastructure and enzyme activity. Plant, Cell & Environment **34,** 1723–1736.

Ocampo G, Koteyeva NK, Voznesenskaya EV, Edwards GE, Sage TL, Sage RF, Columbus JT. 2013. Evolution of leaf anatomy and photosynthetic pathways in Portulacaceae. American Journal of Botany **100,** 2388–2402.

Posada D. 2008. jModelTest: phylogenetic model averaging. Molecular Biology and Evolution **25,** 1253–1256.

Pyankov VI, Artyusheva EG, Edwards GE, Black CC Jr, Soltis PS. 2001. Phylogenetic analysis of tribe Salsoleae (Chenopodiaceae) based on ribosomal ITS sequences: implications for the evolution of photosynthesis types. American Journal of Botany **88,** 1189–1198.

P'yankov V, Voznesenskaya E, Kondratschuk A, Black C. 1997. A comparative anatomical and biochemical analysis in *Salsola* (Chenopodiaceae) species with and without a Kranz type leaf anatomy: a possible reversion of C_4 to C_3 photosynthesis. American Journal of Botany **84,** 597.

Rawsthorne S, Bauwe H. 1998. C_3–C_4 intermediate photosynthesis. In: Raghavendra AS, ed. *Photosynthesis. A comprehensive treatise.* Cambridge: Cambridge University Press, 150–162.

Rawsthorne S, Hylton CM, Smith AM, Woolhouse HW. 1988. Photorespiratory metabolism and immunogold localization of photorespiratory enzymes in leaves of C_3 and C_3–C_4 intermediate species of *Moricandia*. Planta **173,** 298–308.

Rilke S. 1999. Revision der Sektion *Salsola s.l.* der Gattung *Salsola* (Chenopodiaceae). Bibliotheca Botanica **149,** 1–189.

Sage RF. 2004. The evolution of C_4 photosynthesis. New Phytologist **161,** 341–370.

Sage RF, Christin PA, Edwards EJ. 2011. The C_4 plant lineages of planet Earth. Journal of Experimental Botany **62,** 3155–3169.

Sage RF, Khoshravesh R, Sage TL. 2014. From proto-Kranz to C_4 Kranz: building the bridge to C_4 photosynthesis. Journal of Experimental Botany **65,** 3341–3356.

Sage RF, Sage TL, Kocacinar F. 2012. Photorespiration and the evolution of C_4 photosynthesis. Annual Review of Plant Biology **63,** 19–47.

Sage TL, Busch FA, Johnson DC, Friesen PC, Stinson CR, Stata M, Sultmanis S, Rahman BA, Rawsthorne S, Sage RF. 2013. Initial events during the evolution of C_4 photosynthesis in C_3 species of *Flaveria*. Plant Physiology **163,** 1266–1276.

Shomer-Ilan A, Nissenbaum A, Waisel Y. 1981. Photosynthetic pathways and the ecological distribution of the Chenopodiaceae in Israel. Oecologia **48,** 244–248.

Stamatakis A. 2006. RAxML-VI-HPC: maximum likelihood-based phylogenetic analyses with thousands of taxa and mixed models. Bioinformatics **22,** 2688–2690.

Stamatakis A, Hoover P, Rougemont J. 2008. A rapid bootstrap algorithm for the RAxML Web servers. Systematic Biology **57,** 758–771.

Vaidya G, Lohman DJ, Meier R. 2011. SequenceMatrix: concatenation software for the fast assembly of multi-gene datasets with character set and codon information. Cladistics **27,** 171–180.

Volkens G. 1887. *Die Flora der aegyptisch-arabischen Wüste auf Grundlage anatomisch-physiologischer Forschungen.* Berlin: Borntraeger.

Voznesenskaya EV. 1976. Ultrastructure of assimilating organs of some species of the family Chenopodiaceae. II. Botanicheskii Zhurnal **61,** 1546–1557 [In Russian].

Voznesenskaya EV, Artyusheva EG, Franceschi VR, Pyankov VI, Kiirats O, Ku MS, Edwards GE. 2001. *Salsola arbusculiformis*, a C_3–C_4 intermediate in Salsoleae (Chenopodiaceae). Annals of Botany **88,** 337–348.

Voznesenskaya EV, Koteyeva NK, Akhani H, Roalson EH, Edwards GE. 2013. Structural and physiological analyses in Salsoleae (Chenopodiaceae) indicate multiple transitions among C_3, intermediate, and C_4 photosynthesis. Journal of Experimental Botany **64,** 3583–3604.

Voznesenskaya E, Koteyeva NK, Chuong SDX, Ivanova AN, Barroca J, Craven L, Edwards GE. 2007. Physiological, anatomical and biochemical characterization of the type of photosynthesis in *Cleome* species (Cleomaceae). Functional Plant Biology **34,** 247–267.

Voznesenskaya EV, Koteyeva NK, Edwards GE, Ocampo G. 2010. Revealing diversity in structural and biochemical forms of C_4 photosynthesis and a C_3–C_4 intermediate in genus *Portulaca* L. (Portulacaceae). Journal of Experimental Botany **61,** 3647–3662.

Wen Z, Zhang M. 2011. Anatomical types of leaves and assimilating shoots and carbon $^{13}C/^{12}C$ isotope fractionation in Chinese representatives of Salsoleae *s.l.* (Chenopodiaceae). Flora **206,** 720–730.

Wen Z, Zhang M. 2015. *Salsola laricifolia*, another C_3–C_4 intermediate species in tribe Salsoleae *s.l.* (Chenopodiaceae). Photosynthesis Research **123,** 33–43.

Williams BP, Aubry S, Hibberd JM. 2012. Molecular evolution of genes recruited into C_4 photosynthesis. Trends in Plant Science **17,** 213–220.

Winter K. 1981. C_4 plants of high biomass in arid regions of Asia. Occurrence of C_4 photosynthesis in Chenopodiaceae and Polygonaceae from the middle east and USSR. Oecologia **48,** 100–106.